https://doi.org/10.5194/egusphere-2026-2345
Preprint. Discussion started: 21 May 2026

The direct hand of the magnetosphere in controlling small-scale auroral plasma turbulence: Introducing the renormalization group

Magnus F Ivarsen[1,2], Glenn C Hussey[1], Yoshizumi Miyoshi[3], David R Themens[4], Atsuki Shinbori[3], and Shoichiro Yokota[5]

[1]Department of Physics and Engineering Physics, University of Saskatchewan, Saskatoon, Canada
[2]The European Space Agency Centre for Earth Observation, Frascati, Italy
[3]Institute for Space-Earth Environmental Research, Nagoya University, Nagoya, Japan
[4]School of Engineering, University of Birmingham, Birmingham, UK
[5]Department of Earth and Space Science, Osaka University, Toyonaka, Japan

Abstract. Studies of high-latitude plasma turbulence in Earth's upper atmosphere fundamentally focus on the differential response of electrons and ions to strong external electric fields generated during geomagnetic storms. Because ions in the E region are heavy and highly collisional, they remain largely tied to the neutral gas, whereas magnetized electrons undergo rapid $\mathbf{E} \times \mathbf{B}$-drift. Microscopic polarization electric fields are generated when the relative drift velocity between these streaming electrons and the background ions exceeds the local ion-acoustic speed, triggering two-stream plasma instabilities, producing Farley Buneman waves. We propose a new theory that explicitly considers thousands, or millions, of such waves being excited inside a limited volume of space around aurorae, subject to the renormalization group. The resulting theory constitutes an effective field-theory for Farley-Buneman turbulence in the Martin-Siggia-Rose formalism. At the core of this theory is a statistical description of Farley-Buneman waves, where we allow each individual wave to produce a polarization electric field. We treat the sum total of these "micro-fields" that occur inside a turbulent volume as a stochastic variable, or simply noise. That noise, now a thermodynamic property, becomes the basis for anomalous diffusion, and an effective diffusion tensor, and we recover the expression for Bohm diffusion. In support of this theory, we present a large statistical analysis of how auroral electrojet turbulence responds to magnetospheric driving, revealing a clear tendency for the observed number density of turbulent waves to scale linearly with driving power, matching the predictions made by our field theory's overdamped equations of motion. Crucially, the effective field theory offers closed-form calculations of macroscopic transport relations that are uniquely suitable for sub-grid parameterization in space weather modeling, mimicking the success of stochastic parameterization in hydrodynamic Earth-system models. The derivation of these parameterized equations demonstrates how Bohm diffusion arises from a statistical-mechanical treatment of turbulent volumes, at the expense of an explicit treatment of the turbulent cascade. The equations should be investigated further, and in future, they may model the evolution of momentum and energy in numerical treatments of global magnetohydrodynamic circulation, below the scale-sizes normally considered accessible to fast, predictive models.

https://doi.org/10.5194/egusphere-2026-2345
Preprint. Discussion started: 21 May 2026

1 introduction

In Earth's lower ionosphere, collisions between charged particles and neutral molecules become so frequent that the ratio of collision to cyclotron frequency is large enough to demagnetize ions below 120 km and electrons below 80 km. The resulting difference in charge carrier mobility between 80 and 120 km allows strong electric fields in the aurora to drive Hall currents – a reservoir of free energy for electrostatic instabilities (Fejer and Kelley, 1980; Huba et al., 1985). For plasma drifts below around 400 m/s, the Hall currents feature little internal structure, owing to ordinary plasma diffusion.

However, given sufficiently strong electric fields, or, equivalently, sufficiently fast electron drifts, the laminar currents rapidly break up into eddies with sizes that vary across a spectrum. This occurs for imposed drift speeds exceeding the ion acoustic speed, C_s, usually around 400 m/s. This triggers the Farley-Buneman (FB) instability via the ion inertia that is excited by the motion of the irregular structures, driven by the electron plasma ($E \times B$) drift (Farley, 1963; Buneman, 1963). This generates an increase in the overall Joule heating rate through the nonlinear dissipation of electrostatic structures (St-Maurice and Goodwin, 2021), and the dissipation occurs soon after the unstable structures have reached maximum amplitude, having taken as much free energy as possible from the system, thereby bringing the electric field to a point of marginal stability (St.-Maurice and Hamza, 2001). The dissipation comes from the inevitable creation of increasingly important wave electric field components along the magnetic field, which erode the structures (Drexler et al., 2002; Oppenheim and Dimant, 2013) and thereby returns the energy to the particles via acceleration. For very strong ambient Hall currents, the additional heating rate from the energy going through FB waves becomes highly relevant through large increases in the ambient electron temperature above 105 km (Schlegel and St.-Maurice, 1981; St.-Maurice, 1985; St-Maurice et al., 1990; Hamza, 1998; St.-Maurice and Hamza, 2001; St-Maurice and Goodwin, 2021).

The foregoing describes a dynamic and complex conversion of ambient Hall currents into electrostatic energy, as demonstrated through in-situ measurements (Pfaff et al., 1987; Kelley et al., 1986b, a), ground-based radar studies, (St. -Maurice et al., 1989; Foster et al., 1992; Foster and Tetenbaum, 1992) and hybrid fluid- and particle-simulations (Oppenheim et al., 1995, 1996; Oppenheim and Dimant, 2013). Recently, radar studies have also shown that the turbulence is triggered preferentially on the edges of the precipitation regions, (Bahcivan et al., 2006; Huyghebaert et al., 2021) where the electric field intensifies (Fujii et al., 2011; Ivarsen et al., 2024b).

Building on this description of externally driven FB turbulence, we surmise a state of criticality, where the response of the non-laminar electrojets around diffuse aurorae is *saturated*, and the system is forced into an overdamped state. To capture the saturation dynamics, we adopt a formalism consistent with Hamza and St-Maurice (1993) and St.-Maurice and Chau (2016): *(1)* the relevant driving term for FB turbulence is controlled by a Doppler-shifted eigenfrequency $\omega' = \omega - \mathbf{k} \cdot \mathbf{V}_d$ that plays an important role after we consider that *(2)* the FB instability itself is regulated by an effective damping term, γ_{eff}, which forces the growth rate to go from large at early stages where the structures are unstable, to zero when the wave is damped to saturation. After that, the growth rate of single structures goes to zero owing to the nonlinear association of the wave field with the perturbed density, in reaction at first (St.-Maurice and Hamza, 2001). In their final stage of evolution, the growth of the wave-field, along the magnetic field, damps the unstable structures and dissipates them.

https://doi.org/10.5194/egusphere-2026-2345
Preprint. Discussion started: 21 May 2026

In specific terms, the dynamics of the density fluctuations in the frame of the drifting plasma are governed by a dispersion relation, that favors growth at first and then becomes highly dissipative, all through the changes in the nonlinear evolution of the eigenfrequency, as given by, e.g., Hamza and St-Maurice (1993),

$$\omega^2 - k_\perp^2 C_s^2 + i\omega' \gamma_{\text{eff}} = 0, \tag{1}$$

where $k_\perp$ is the perpendicular wavenumber and γ_{eff} is large, owing to the small magnitude of Pedersen currents relative to electron Hall currents. Once we recognize the impacts of the non-linear effects exerted on the eigenfrequencies, the dynamics becomes quite complex. The large value of γ_{eff} forces ω' to remain very close to zero, so that the frequency remains locked at $\mathbf{k} \cdot \mathbf{V}_d$. The complexity emerges from the fact that $\mathbf{V}_d$ responds nonlinearly to wave amplitudes, and ends up being a function of time. The term $\omega^2 - k_\perp^2 C_s^2$ in individual structures therefore fluctuates between positive and negative. The system then sees repeated oscillating cycles occurring in intensely excited, limited volumes of space. From this complexity we observe the emergence of novel qualities.

1.1 The role of emergence

However, the exact meaning of this fact is difficult to define, as it is unclear whether or not statistical qualities that emerge in complex datasets exist in a directly observable sense. We are faced with two interpretations. ***(1)*** Under the assumption of *strong* emergence, statistically derived qualities are rigorously replicated in nature, arising uniquely through collective interaction, and this interpretation is usually confined to condensed matter physics (Drossel, 2021) and chemistry. ***(2)*** On the other hand, in the case of *weak* emergence, the statistically derived qualities are observable only in aggregate, and represent a descriptive, working mode of explaining complex phenomena.

In the present paper, we present a clear case of emergence from the complex interactions of FB turbulence, though we are unable to determine whether this result should be interpreted through the lens of strong emergence, and so we favour a weak interpretation. The result is arrived at through renormalization group (RG) theory, and we demonstrate that this theoretical application is entirely consistent with observations in statistical aggregates. Under a hypothetical strong interpretation, this would imply that the turbulent ionosphere features noise-enabled transport of momentum and energy, a transport that is observable in statistical aggregates. The question becomes whether this transport of momentum and energy adheres to a set of defined macroscopic laws. We define such a macroscopic effective field theory, wherein a deterministic advection-diffusion equation allows for parametrized transport equations (Eq. 2 below), for dynamics smaller than around 100 km in cross-field scale-size.

We favour a weak interpretation, for merits that we shall soon espouse, and urge further research into the thermosphere-ionosphere-magnetosphere interaction through the lens of complexity.

Numerical magnetohydrodynamic solutions of the magnetosphere–ionosphere system are unable to resolve scales smaller than approximately 50–100 km, set by the computational cost of global fluid solvers (Wiltberger et al., 2017a, b). Below this "grid-cell"-scale, electrojet turbulence must be evaluated using expensive hybrid fluid-kinetic simulations (Oppenheim et al., 1995; Dimant and Sudan, 1995; Dimant et al., 2021), and the nature and magnitude of the turbulent cascade in this regime remain unknown in operational space weather forecasting, and replacements are found in terms of eddy diffusion (Wu et al., 2017,

https://doi.org/10.5194/egusphere-2026-2345
Preprint. Discussion started: 21 May 2026

e.g.). This problem is echoed in recent history, in terrestrial weather and climate modeling, where sub-grid convective processes are likewise inaccessible to direct simulation. The atmospheric community has addressed this gap through two generations of parameterization: deterministic effective diffusion (Smagorinsky, 1963) and, more recently, stochastic parameterization that treats unresolved convective scales as noise, yielding demonstrable improvements in ensemble forecast skill (Palmer, 2012; Berner et al., 2017). No comparable framework currently exists for sub-grid electrojet turbulence in space weather models. In what follows, we construct one. We treat the sum total of polarization electric fields produced by individual Farley–Buneman waves as a stochastic variable, and we apply renormalization group theory, yielding closed-form transport coefficients – an effective diffusion tensor (Eq. 2) and an anomalous resistivity (Eq. 51) – that parameterize the sub-grid turbulent cascade in three dimensions. These relations are suitable for direct incorporation into global magnetohydrodynamic models as constitutive transport laws, and provide strong motivation for our investment in the *weak*, i.e., descriptive, interpretation of our field-theory.

1.2 Summary of the effective Farley-Buneman field theory

This paper is oriented around an effective field theory for electrojet turbulence. In this formulation, the spatial dynamics are governed by an effective diffusion tensor,

$$\mathbf{D}_{\text{eff}} = \gamma_{\text{eff}}^{-1}(C_s^2\,\mathbb{I} - \mathbf{V}_d \otimes \mathbf{V}_d), \tag{2}$$

where C_s is the acoustic speed and $\mathbf{V}_d$ is the saturating drift velocity. Here, the instability manifests as negative diffusion (Ashinsky, 1988) instead of wave-growth, triggered when drifts surpass the ion acoustic speed ($D_{\parallel} \sim C_s^2 - V_d^2 < 0$). This unstable growth occurs only along the mean drift, while transverse modes, the overdamped secondary waves, (Hamza and St-Maurice, 1993) remain subject to positive effective diffusion $D_{\perp} \sim C_s^2$. The instability grows until it reduces the driving field $\mathbf{V}_d$, flipping the diffusion from negative to positive and ensuring marginal stability.

Solving the resulting advective-diffusive equation of motion for the renormalized FB waves yields an Adler-Ohmic bifurcation in the system, where magnetospheric forcing elicits a linear (Ohmic) response in the degree of proliferation of FB turbulence. We demonstrate the validity of the theory by showing that, during intense diffuse aurorae, the ionosphere-magnetosphere coupling exhibits the theorized Adler-Ohmic bifurcation, (Adler, 1946) with an Ohmic response where E-region turbulence intensity n scales linearly with electromagnetic power input: $n \propto \Delta E$, but will only do so when ΔE exceeds a characteristic threshold wave power ΔE_c, measured by the Arase spacecraft (Miyoshi et al., 2018b, 2022), We predict that the linear relationship follows from the saturation of wave amplitude. The saturation of amplitudes forces the number of turbulent parcels (proliferation) to track the driver. The ionosphere around diffuse aurorae thus self-organizes into a driven-dissipative boundary, preserving a scaled-down structural imprint of the magnetospheric boundary turbulence, while optimizing energy dissipation.

2 Methodology

ICEBEAR is an auroral coherent radar that observed three-meter Farley-Buneman waves near the radar's horizon (Huyghebaert et al., 2019; Lozinsky et al., 2022), where those waves are perpendicular to the beamed radar signal. Echoes produced when the

https://doi.org/10.5194/egusphere-2026-2345
Preprint. Discussion started: 21 May 2026

radar signal is Bragg-like-scattered by the Farley-Buneman waves, and a local analysis of the echo characteristics, correspond directly to a quantitative description of Farley-Buneman turbulence. The radar can record thousands of echo locations per second, yielding exceedingly large point-cloud datasets (Ivarsen et al., 2023, 2024c). ICEBEAR combines software-defined radio with multiple frequency interferometry, which allows the radar to observe the bulk 3D shapes of the turbulent ionosphere near aurorae.

The radar operates every night near Saskatoon in Saskatchewan, Canada, regardless of the ongoing geomagnetic activity, and it only observes auroral plasma turbulence during approximately 4% of the time spent operational. However, it observes the turbulent trails of *meteors* that burn up in Earth's atmosphere at all times, meaning that an ICEBEAR dataset in aggregate yields a statistical treatment of an *entire space weather system*. The transition from a static state, where the only observable turbulence stems from the perpetual rain of meteors into Earth's atmosphere, to a fully turbulent state wherein the aurora is *intermittently injecting* free energy that drives intense small-scale plasma turbulence (Ivarsen et al., 2024b).

In this paper, we shall analyze such a space weather system through a large database of observations by the ICEBEAR radar and the Japanese inner-magnetosphere spacecraft Arase (Miyoshi et al., 2018b, 2022) Arase's orbit features an apogee of 32,000 km, a perigee of 400 km, an inclination angle of 31°, and an orbital period of 570 minutes. We collected data from instances where both instruments were operational, and both were inside the nightside auroral region. This exercise yields 270 million radar echo detections and some 500,000 electric field wave spectra observed by Arase, covering such frequencies that are known to interact with electrons causing particle precipitation.

A theoretical (renormalization group flow) and data-driven analysis converge on the existence of an emergent regime in auroral plasma turbulence, wherein FB waves in ensemble produce a *noise variable*, one that translates directly to Bohm diffusion. This important result highlights the utility of complexity science to characterize space weather on scales below the typical "grid cell" of a global magnetohydrodynamic model.

2.1 Renormalization group theory

In Section 1.1, we described emergence in complex systems, namely that order can emerge from otherwise efficiently dissipative processes, planting modes of fluctuation into a space weather system that are not predictable from deterministic theory alone, but rather completely dependent on a probabilistic treatment of an *ensemble*, whose sum total is unpredictable from an isolated analysis of a single constituent process.

The foregoing represents a feedback mechanism that is completely missed by any theoretical analysis of the individual processes in isolation, and therefore we note the distinct merit to a confirmed observation of large-scale emergent behaviour in the statistical treatment of space weather systems around diffuse aurorae, the topic of the present paper. This observation justifies the construction of an effective field theory for auroral plasma turbulence, a step that decidedly acknowledges the vast complexity that is being renormalized in such a construct. The potential feedback asserted by this renormalized complexity is the precise justification for the drastic step.

Having assiduously justified the step, we perform a Martin-Siggia-Rose (MSR) renormalization group (RG) theoretical deconstruction (Wilson, 1971; Hohenberg and Halperin, 1977) of Farley-Buneman turbulence, treating polarization electric

https://doi.org/10.5194/egusphere-2026-2345
Preprint. Discussion started: 21 May 2026

fields produced by FB wave saturation (i.e., waves very briefly coasting at the ion sound speed), as a stochastic ensemble. As we shall demonstrate, the stochastic variable is directly renormalized into an anomalous transport coefficient, where we recover Bohm diffusion. This entails treating FB turbulence as *noise*, and that the effects of this noise necessitate a non-linear dynamic synchronization treatment of auroral plasma turbulence. We deduce from this observation that the noise is organized in a particular synchronization pattern, one that is irreducible from a fluid or kinetic, i.e., theoretical, treatment of FB turbulence. By this, we mean that the overall pattern is created by numerous on-off trigger behaviours, cleanly describable by Kuramoto synchronization in terms of Josephson junctions (microelectrical superconductor chips).

In what follows, we construct an effective action in the path integral formalism, using the Martin-Siggia-Rose framework, and with this, we perform a dynamic scaling analysis with spatial rescaling $x' = b^{-1}x$ and temporal rescaling $t' = b^{-z}t$. We then derive the macroscopic "Adler-Ohmic" linear power law observed in the auroral E-region ionosphere, from the microscopic physics of FB turbulence. The derivation is performed in the neutral atmosphere's frame of reference, but an equivalent derivation in the ions' frame of reference yields identical results.

2.1.1 The dispersion relation

We write out the dispersion relation in the atmosphere frame, defining the wave frequency ω relative to the neutral gas,

$$\omega^2 - k_\perp^2 C_s^2 + i(\omega - \mathbf{k}\cdot\mathbf{V}_{d0})\gamma_{\text{eff}} = 0, \tag{3}$$

where $\mathbf{V}_{d0}$ is the mean $\mathbf{E}\times\mathbf{B}$ drift velocity. We note that the real part of the frequency corresponds to the convective derivative in the time domain, while the imaginary damping term acts on the Doppler-shifted frequency.

Next, we shall apply the Martin-Siggia-Rose formalism of describing statistical dynamics for classical systems (Phythian, 1976; Andersen, 2000), turning the stochastic differential equations of motion for our system into an effective, macroscopic field theory (Bonicelli et al., 2025). We start by constructing the unperturbed action in the path integral formalism, based on Eq. (3). In the neutral gas frame, this explicitly retains the mean advection of the plasma structures:

$$S_0 = \int dt\, d^d x\, \tilde{\psi}\left[\partial_t^2 + 2(\mathbf{V}_{d0}\cdot\nabla)\partial_t + (\mathbf{V}_{d0}\cdot\nabla)^2 - C_s^2\nabla^2 + \gamma_{\text{eff}}(\partial_t + \mathbf{V}_{d0}\cdot\nabla)\right]\psi, \tag{4}$$

where $\psi = \delta N_e/N_{e,0}$ is the electron density variation divided by mean density, and $\tilde{\psi}$ is the auxiliary response field acting as a Lagrange multiplier to enforce the deterministic trajectory (Bonicelli et al., 2025). A two-step argument treats the non-linearities in the turbulent plasma:

(1) The linear propagator S_0 accounts for the mean flow but neglects the effects of turbulent mode-coupling. However, the physical mechanism at the level of individual structures involves the development of secondary polarization fields. A justification for treating these non-linearities stochastically can be derived from the work of St.-Maurice and Hamza (2001); Drexler et al. (2002). Based on Fourier analysis, St.-Maurice and Hamza (2001) showed that for an initial finite-size structure, polarization electric fields are created that oppose the driving field. These internal fields saturate the instability locally, explaining why VHF Doppler speeds cluster around C_s (Figure 3b).

https://doi.org/10.5194/egusphere-2026-2345
Preprint. Discussion started: 21 May 2026

(2) As a result of point *(1)*, we construct a stochastic source term driven by these self-generated polarization fields. Rather than a slow modulation, we recognize that the total drift velocity $\mathbf{V}(x,t)$ at any point is the sum of the coherent mean drift $\mathbf{V}_{d0}$ and a fluctuating component $\delta\mathbf{v}(t)$ arising from the turbulent ensemble:

$$\mathbf{V}(x,t) = \mathbf{V}_{d0} + \delta\mathbf{v}(x,t). \tag{5}$$

Because these fluctuations are driven by the instability itself, they occur on fast timescales, and we write the time-dependent drift for an individual structure i as

$$\mathbf{V}_i(t) = \mathbf{V}_{d0}\left[1 - \varepsilon\sin(\Omega t + \alpha_i)\right], \tag{6}$$

where Ω represents the waves' life-cycle, α_i represents the random phase of the i^{th} structure, and ε is the amplitude of the non-linear feedback. Furthermore, since the macroscopic turbulent electrojet is an ensemble of such structures spread over 10s of km, the phase information of the fluctuations is effectively random across the volume. We therefore define the stochastic velocity field $\delta\mathbf{v}(x,t)$ via the random phase approximation (RPA) (Krommes, 2002),

$$\delta\mathbf{v}(x,t) = -\varepsilon\sum_i \mathbf{v}_i\sin(\Omega t + \alpha_i(x)). \tag{7}$$

By virtue of the central limit theorem, the sum of these uncorrelated, fast-oscillating terms converges to a Gaussian random variable. Thus, we formally replace the deterministic non-linear trajectory with a stochastic field $\delta\mathbf{v}$ governed by a Gaussian probability distribution $P[\delta\mathbf{v}]$,

$$P[\delta\mathbf{v}] \propto \exp\left(-\int dt\, d^dx \frac{|\delta\mathbf{v}|^2}{2\sigma_v}\right). \tag{8}$$

Here, the variance σ_v is constrained by the power of the turbulent electric fields. Following the MSR formalism, this stochastic noise enters the equation of motion as a multiplicative source term acting on the gradient of the density field,

$$\hat{\mathcal{L}}_0\psi = -\gamma_{\text{eff}}(\delta\mathbf{v}\cdot\nabla)\psi, \tag{9}$$

which introduces a linear coupling between the response field $\tilde{\psi}$ and the noise ensemble,

$$S_{\text{coupling}} = \int dt\, d^dx\, \tilde{\psi}\left[\gamma_{\text{eff}}(\delta\mathbf{v}\cdot\nabla)\psi\right]. \tag{10}$$

To derive the effective macroscopic action, we integrate over the ensemble of phase histories. We compute the expectation value of the coupling term over the Gaussian distribution,

$$I = \left\langle \exp\left(i\int dt\, d^dx\,(\gamma_{\text{eff}}\tilde{\psi}\nabla\psi)\cdot\delta\mathbf{v}\right)\right\rangle_{\delta\mathbf{v}}. \tag{11}$$

Using the Gaussian integral identities, we obtain,

$$I = \exp\left(-\frac{\sigma_v}{2}\int dt\, d^dx\left(\gamma_{\text{eff}}\tilde{\psi}\nabla\psi\right)^2\right). \tag{12}$$

https://doi.org/10.5194/egusphere-2026-2345
Preprint. Discussion started: 21 May 2026

The MSR path integral weight is defined as $\mathcal{Z} = \int \mathcal{D}\psi\mathcal{D}\tilde{\psi}\, e^{iS}$. To translate the real-valued Gaussian probability weight of the noise fluctuations into the complex-weighted path integral formalism, we identify the integration result with iS_{int}, the imaginary component of the action,

$$iS_{\text{int}} = -\frac{\sigma_v}{2}\gamma_{\text{eff}}^2 \int dt\, d^d x\, (\tilde{\psi}\nabla\psi)^2. \tag{13}$$

It is crucial to note the specific mechanics of scale separation at play here. Unlike standard Wilsonian renormalization, which relies on spatial momentum-shell integration to explicitly eliminate fast, high-wavenumber fluctuation modes, our MSR approach achieves scale separation primarily in the time domain. This Gaussian path integral over the random temporal phase histories mathematically transforms the microscopic polarization feedback directly into a macroscopic anomalous diffusion tensor, bypassing the need for explicit k-space integration.

We can now combine the deterministic propagator (derived from the dispersion relation, Eq. 3), and the stochastic noise term, (Eq. 13), obtaining the total action,

$$S = \int dt, d^d x \left\{ \tilde{\psi}\left[\partial_t^2 + 2(\mathbf{V}_{d0}\cdot\nabla)\partial_t + (\mathbf{V}_{d0}\cdot\nabla)^2 - C_s^2\nabla^2 + \gamma_{\text{eff}}(\partial_t + \mathbf{V}_{d0}\cdot\nabla)\right]\psi + i\frac{\sigma_v}{2}\gamma_{\text{eff}}^2(\tilde{\psi}\nabla\psi)^2 \right\} \tag{14}$$

2.1.2 Renormalization group flow

We determine the macroscopic phase of the system by analyzing the flow of the coupling constants under a rescaling of spacetime,

$$x \to bx,$$
$$t \to b^z t,$$
$$\psi \to b^\chi \psi,$$
$$\tilde{\psi} \to b^{\tilde{\chi}}\tilde{\psi}.$$

The integration measure therefore transforms as,

$$\int dt\, d^d x \to b^{z+d} \int dt\, d^d x. \tag{15}$$

We next choose the stiffness operator (diffusion) to be scale-invariant. In other words, with the scaling relations applied to $C_s^2\tilde{\psi}\nabla^2\psi$ (Eq. 24), we obtain the constraint,

$$\chi + \tilde{\chi} = 2 - z - d. \tag{16}$$

https://doi.org/10.5194/egusphere-2026-2345
Preprint. Discussion started: 21 May 2026

Applying this constraint to the other operators in the action to find their scaling behavior relative to the stiffness, we find that,

$$\int dt\, d^d x\, \tilde{\psi}\partial_t^2\psi \;\sim\; b^{(2-z-d)+z+d-2z} = b^{2-2z}, \tag{17}$$

$$\int dt\, d^d x\, \gamma_{\text{eff}}\tilde{\psi}\partial_t\psi \;\sim\; b^{(2-z-d)+z+d-z} = b^{2-z}, \tag{18}$$

$$\int dt\, d^d x\, \gamma_{\text{eff}}\tilde{\psi}(\mathbf{V}_{d0}\cdot\nabla)\psi \;\sim\; b^{(2-z-d)+z+d-1} = b^{1}, \tag{19}$$

$$\int dt\, d^d x\, \tilde{\psi}(\mathbf{V}_{d0}\cdot\nabla)^2\psi \;\sim\; b^{z+d+\chi+\tilde{\chi}-2} = b^{0}, \tag{20}$$

$$\int dt\, d^d x\, \frac{\sigma_v}{2}\gamma_{\text{eff}}^2(\tilde{\psi}\nabla\psi)^2 \;\sim\; b^{z+d-2+2(\chi+\tilde{\chi})} = b^{2-z-d}, \tag{21}$$

where we used Eq. (16). We observe that at the inertial fixed point ($z = 1$), the inertial term (Eq. 17) is relevant. However, with increasing z the system flows to the dissipative fixed point at $z = 2$, where the inertial term becomes irrelevant (b^{-2}) and the damping term becomes marginal (b^0). Crucially, the linear advection term (Eq. 19) scales as b^1, identifying it as a relevant operator: macroscopic transport is dominated by the mean drift.

In the macroscopic limit, the inertial terms (∂_t^2) and the stochastic driver fluctuations (σ_v) are renormalized. The stochastic variance σ_v generates the anomalous diffusion tensor, while the mean drift remains as a relevant transport term. This leaves a deterministic effective theory describing an advecting, diffusing fluid,

$$S = \int dt\, d^d x\tilde{\psi}\left[\gamma_{\text{eff}}(\partial_t + \mathbf{V}_{d0}\cdot\nabla) + (\mathbf{V}_{d0}\cdot\nabla)^2 - C_s^2\nabla^2\right]\psi. \tag{22}$$

At this point, we reinstate the internal feedback reaction that the unstable structures excite (St.-Maurice and Hamza, 2001), namely that the turbulent electric field is periodically brought down to the threshold,

$$\mathbf{V}_{d0} \to \mathbf{V}_d = \mathbf{V}_{d0}\left(1 - \tilde{\alpha}\langle|\psi|\rangle^2\right), \tag{23}$$

where we recognize that the variance of the microscopic velocity fluctuations (σ_v) manifests macroscopically as an anomalous drag force. The importance of this step is considerable, and it is equally important to point out that this step, that bringing the electric field back to the instability threshold is governed by amplitude saturation ($\langle|\psi|\rangle^2$) is *firmly supported in the literature* (St.-Maurice and Hamza, 2001).

A self-regulating feedback mechanism follows: as the turbulent amplitudes increase, the driving electric field is brought down towards the threshold velocity, the ion acoustic speed, C_s, which in turn kills the instability and lowers the turbulent amplitude ($\langle|\psi|\rangle^2 \to 0$). As we shall demonstrate, this description ensures that the system finds the fixed point where the effective drift is just above the ion acoustic speed (Figure 3b), and this is likewise strongly supported in the literature (Foster and Erickson, 2000; Oppenheim and Dimant, 2013; Koustov et al., 2005; Chau and St.-Maurice, 2016). We obtain the deterministic action,

$$S = \int dt\, d^d x\tilde{\psi}\left[\gamma_{\text{eff}}(\partial_t + \mathbf{V}_d\cdot\nabla) - (\mathbf{V}_d\cdot\nabla)^2 - C_s^2\nabla^2\right]\psi. \tag{24}$$

Here, we can combine the two stiffness terms by way of tensor notation,

$$\left[(\mathbf{V}_d\cdot\nabla)^2 - C_s^2\nabla^2\right]\psi = -\nabla\cdot\left(C_s^2\mathbb{I} - \mathbf{V}_d\otimes\mathbf{V}_d\right)\cdot\nabla\psi, \tag{25}$$

https://doi.org/10.5194/egusphere-2026-2345
Preprint. Discussion started: 21 May 2026

which allows us to write the first-order, overdamped advection-diffusion equation,

$$S_{\text{eff}} = \int dt\, d^d x\, \tilde{\psi}\, \gamma_{\text{eff}} \left[(\partial_t + \mathbf{V}_d \cdot \nabla) - \gamma_{\text{eff}}^{-1} \nabla \cdot \left(C_s^2 \mathbb{I} - \mathbf{V}_d \otimes \mathbf{V}_d \right) \cdot \nabla \right] \psi. \tag{26}$$

We note that the spatial dynamics are governed by the effective diffusion tensor $\mathbf{D}_{\text{eff}} = \gamma_{\text{eff}}^{-1}(C_s^2\mathbb{I} - \mathbf{V}_d \otimes \mathbf{V}_d)$, with $\mathbf{V}_d$ representing the saturated drift,

$$\mathbf{D}_{\text{eff}} = \frac{1}{\gamma_{\text{eff}}} \begin{bmatrix} C_s^2 - V_d^2 & 0 & 0 \\ 0 & C_s^2 & 0 \\ 0 & 0 & C_s^2 \end{bmatrix}. \tag{27}$$

(1) In directions parallel to the mean advection $\mathbf{V}_{d0}$, if the driving drift $V_{d0} > C_s$, the effective diffusion coefficient becomes *negative*, which we identify as the macroscopic signature of the instability. This is followed by saturation,

$$D_{\parallel}(\psi) \approx (C_s^2 - V_{d0}^2) + 2\tilde{\alpha} V_{d0}^2 |\psi|^2, \tag{28}$$

where we have linearized the effective drift squared ($V_d^2 \approx V_{d0}^2 - 2\tilde{\alpha} V_{d0}^2 |\psi|^2$) and neglected higher-order $\mathcal{O}(|\psi|^4)$ terms. The negative diffusion that commences when $V_{d0} > C_s$ leads to perturbation growth, which in turn activates the anomalous drag (saturation) through $|\psi|^2$, stabilizing the transport.

(2) In directions perpendicular to the drift, the diffusion simplifies to $\mathbf{D}_{\text{eff}} \approx C_s^2$, the transverse terms representing the ordinary diffusion of the transverse modes. These act as an energy sink, aligning with Hamza and St-Maurice (1993), who explicitly identified the mode-coupled secondary waves as acting akin to "driven, overdamped oscillators."

2.1.3 Advective-diffusive dynamics

The foregoing subsection established that at macroscopic scales ($z = 2$), the inertial terms (∂_t^2) are irrelevant. The system flows universally to an advective-diffusive state, and so we write the effective equation of motion for the turbulent density fluctuation field $\psi(\mathbf{x}, t)$ as,

$$\gamma_{\text{eff}} \left(\frac{\partial}{\partial t} + \mathbf{V}_{d0} \cdot \nabla \right) \psi - \nabla \cdot \left[(C_s^2 - V_{d0}^2) + 2\tilde{\alpha} V_{d0}^2 |\psi|^2 \right] \cdot \nabla \psi = S(\mathbf{x}, t), \tag{29}$$

where γ_{eff} is the renormalized effective damping. $S(\mathbf{x}, t)$ is a source term, which we decompose into an amplitude $\mathcal{E}$ and a phase $\theta(t)$,

$$S(\mathbf{x}, t) = \mathcal{E}\, e^{i(\mathbf{k}\cdot\mathbf{x} - \theta(t))}, \tag{30}$$

where $\mathcal{E}$ is the strength of the driver and θ is phase. Here, we consider the VHF radar's (and the instability's) natural preference for the driving modes that resonate with the ion acoustic speed. To account for this observational effect, we approximate the driver phase speed with the acoustic speed characteristic of the saturated state,

$$\dot{\theta} \approx k C_s. \tag{31}$$

https://doi.org/10.5194/egusphere-2026-2345
Preprint. Discussion started: 21 May 2026

We next express the turbulent plasma density field ψ in terms of a slowly varying amplitude $A(t)$ and phase $\phi(t)$:

$$\psi(\mathbf{x},t) = A(t)\, e^{i(\mathbf{k}\cdot\mathbf{x}-\phi(t))}. \tag{32}$$

We substitute Eqs. (30) and (32) into the effective equation of motion. The convective derivative on the left-hand-side expands as,

$$\left(\frac{\partial}{\partial t} + \mathbf{V}_d\cdot\nabla\right)\psi = \left[(\dot{A} - iA\dot{\phi}) + iA(\mathbf{k}\cdot\mathbf{V}_d)\right] e^{i(\mathbf{k}\cdot\mathbf{x}-\phi)}. \tag{33}$$

Combining this with the diffusion term,

$$-\nabla\cdot\mathbf{D}_{\text{eff}}\cdot\nabla\psi = \left(\lambda_0 + \tilde{\alpha}V_{d0}^2|\psi|^2\right)\psi, \tag{34}$$

where λ_0 is the positive, renormalized, anomalous diffusion coefficient, representing the effective macroscopic damping at the stable, dissipative fixed point (post-saturation), and where we neglect higher-order non-linear interaction terms. With Eq. (30), the full macroscopic equation of motion reads,

$$\left[\dot{A} - iA(\dot{\phi} - \mathbf{k}\cdot\mathbf{V}_d)\right] + \lambda_0 A = \mathcal{E}(\cos\Theta + i\sin\Theta). \tag{35}$$

where we defined the phase mismatch $\Theta(t) \equiv \phi(t) - \theta(t)$. Finally, Eq. (35) can be expressed more sensibly by recognizing that,

$$\dot{\phi} - \mathbf{k}\cdot\mathbf{V}_d = \dot{\Theta} + \dot{\theta} - \mathbf{k}\cdot\mathbf{V}_d \approx \dot{\Theta} - k(V_d - C_s), \tag{36}$$

which, when substituted this into Eq. (35), yields the final, macroscopic equation of motion,

$$\left[\dot{A} - iA\left(\dot{\Theta} - k(V_d - C_s)\right)\right] + \lambda_0 A = \mathcal{E}(\cos\Theta + i\sin\Theta). \tag{37}$$

(1) The imaginary part of Eq. (37) reveals the phase dynamics relative to the mean flow.

$$-A\left[\dot{\Theta} - k(V_d - C_s)\right] = \mathcal{E}\sin\Theta, \tag{38}$$

which we can rearrange to isolate $\dot{\Theta}$, yielding the Adler equation for phase-locking phenomena, (Adler, 1946; Ambegaokar and Halperin, 1969; Wiesenfeld, 1996)

$$\dot{\Theta} = k(V_d - C_s) - \frac{\mathcal{E}}{A}\sin\Theta. \tag{39}$$

(2) Taking the real part of Eq. (37) yields,

$$\dot{A} + \lambda_0 A = \mathcal{E}\cos\Theta, \tag{40}$$

which we can solve for the steady state by applying singular perturbation theory (Jones, 1995). The characteristic lifetime of FB turbulence is *short*, on millisecond timescales (< 1 s), while the driver $\mathcal{E}$ varies over seconds, enabling us to write $\epsilon = \tau/T_{\text{driver}} \ll 1$. In the limit $\epsilon \to 0$, the time derivative $\epsilon\dot{A}$ vanishes. The system collapses onto the slow manifold,

$$A(t) \approx \frac{\mathcal{E}}{\lambda_0}\cos\Theta(t). \tag{41}$$

https://doi.org/10.5194/egusphere-2026-2345
Preprint. Discussion started: 21 May 2026

To relate this to the radar observations, we approximate the echo intensity n with the turbulence power, or the time-averaged square of the amplitude, $n = \langle A^2 \rangle_t$. Squaring Eq. (41) and time-averaging over the rapid phase slippage (where $\langle \cos^2 \Theta \rangle = 1/2$), we find that the turbulence intensity becomes proportional to the square of the driver strength,

$$n \propto \frac{1}{2\lambda_0^2} \mathcal{E}^2. \tag{42}$$

Since the source term $\mathcal{E}^2$ is proportional to the input wave power ΔE, this strictly recovers the Adler-Ohmic regime observed in Figure 3c): the turbulence intensity scales linearly with the driving power, confirming that the complex microscopic physics linearize in the macroscopic view of the system.

2.1.4 The cross-over scale

From Eq. (39), we define the phase-locking criterion,

$$|k(V_d - C_s)| \leq \frac{\mathcal{E}}{A}, \tag{43}$$

yielding the stability bandwidth. We derive the crossover-scale L_c separating the inertial drift regime from the macroscopic effective field theory. We utilize the slow-manifold solution to the amplitude equation, $A = \mathcal{E}/(\sqrt{2}\lambda_0)$. Substituting the renormalized diffusive linewidth $\lambda_0 = D_{\text{eff}} k^2$ into Eq. (43) yields the scale-dependent locking condition:

$$k(V_d - C_s) \leq \sqrt{2} D_{\text{eff}} k^2. \tag{44}$$

We solve for the critical wavenumber k_c, the minimum k required for the diffusive damping (right-hand-side) to overcome the linear drift drive (left-hand side):

$$k_c = \frac{V_d - C_s}{\sqrt{2} D_{\text{eff}}}, \tag{45}$$

corresponding to the cross-over scale for the RG flow,

$$L_c = \frac{2\sqrt{2}\pi D_{\text{eff}}}{V_d - C_s}. \tag{46}$$

This length scale demarcates the validity of the effective field theory. For small scales ($L < L_c$), the renormalized diffusion dominates, and the system is described by the macroscopic transport. In other words, the system's macroscopic correlation length is characteristic of a continuous phase transition, (Hohenberg and Halperin, 1977) diverging at $V_d = C_s$.

3 Results

In this section, we shall present results form case studies and from a large statistical aggregate, that directly support the foregoing description. First, we shall recount the nature of the particle precipitation found in the diffuse aurorae.

The kinetic energy of the particle precipitation in diffuse and pulsating auroral patches, created when wave-particle interactions leads to pitch-angle scattering of hot electrons in Earth's radiation, or Van Allen, belts, (Thorne et al., 2010; Kasahara

https://doi.org/10.5194/egusphere-2026-2345
Preprint. Discussion started: 21 May 2026

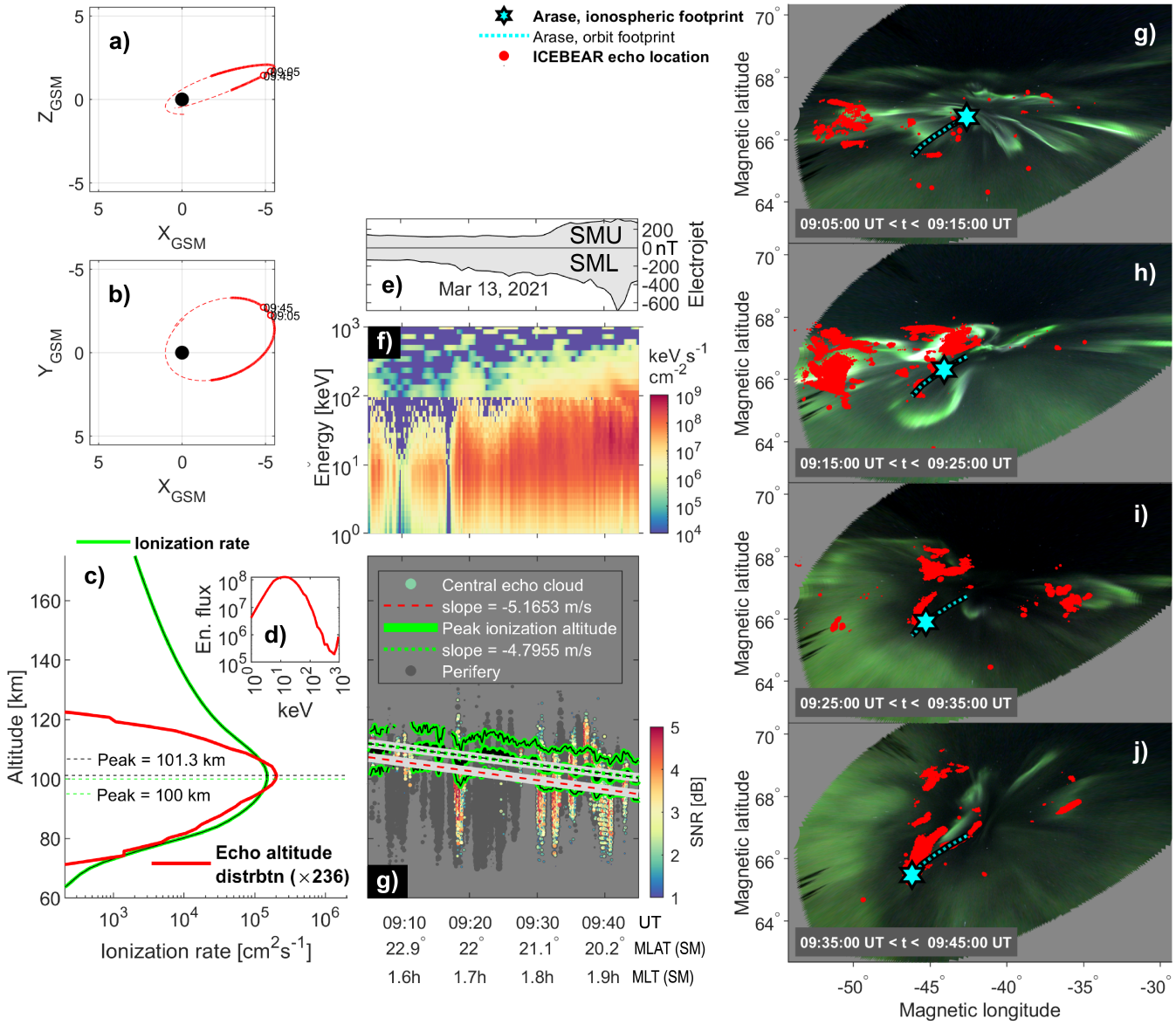

Figure 1. Panels a) and b) show Arase's position in the magnetosphere during the conjunction, in units of Earth radii. **Panel c)** compares the inferred ionization altitude profile from Arase (green), based on the accumulative precipitating energy flux through the interval, with the altitude distribution of radar echoes superposed (red line). **Panel d)** shows the median precipitating electron spectra, while **Panel e)** shows the upper and lower envelope of the auroral electrojet index. **Panel f)** shows the combined precipitating electron energy flux. **panel g)** show altitude-time-intensity point-clouds of echoes, color-coded by signal-to-noise ratio (SNR). Green and black lines indicate the peak ionization altitude (thick line) and a single standard deviation (thin lines). Echoes colored dark grey are observed outside of the radar's central field-of-view, whose altitudes are anomalous (Ivarsen et al., 2023). **Panels g–j)** show auroral images from the TREx RGB (Gillies et al., 2020) all-sky-imager at Rabbit Lake, with radar echo locations in red and Arase's ionospheric footprint as a cyan star.

https://doi.org/10.5194/egusphere-2026-2345
Preprint. Discussion started: 21 May 2026

et al., 2018a) can be high. Significant precipitation is found even at energies larger than 30 keV (Nishimura et al., 2020), and Arase frequently observes significant particle fluxes approaching 1 MeV. This ionizes the ionosphere at low altitudes (Fang et al., 2010; Miyoshi et al., 2015, 2021), where the FB instability may become modulated by ohmic wave-heating (Dimant and Sudan, 1997; St.-Maurice and Chau, 2016) and the electron thermal instability (Dimant and Oppenheim, 2004; Dimant, 2024), as well as conventional FB waves, meaning electrojet turbulence will effectively accompany particle precipitation throughout the E-region; this is the radio, or radar, aurora.

Figure 1 shows measurements that confirm the foregoing, performed during the onset of a magnetospheric substorm, which was captured by a conjunction between the 3D VHF radar ICEBEAR and the inner-magnetosphere spacecraft Arase (Miyoshi et al., 2018a, b). Notably, during this direct conjunction lasting 40-minute interval, we observe a clear and unequivocal relation between the estimated precipitating particle flux and the spatiotemporal distribution of auroral plasma turbulence.

We combine the electron particle detector data through the LEP-e, (Kazama et al., 2017) MEP-e, (Kasahara et al., 2018b) and HEP (Mitani et al., 2018) instruments onboard Arase, and we constrain the data to pitch-angles lower than 5° (LEP-e, MEP-e) and 10° (HEP), which we take as a proxy for the real precipitating energy flux. We convert this flux to an ionization rate altitude profile following Ivarsen (2026), and we compare this ionization altitude profile to the altitude-distribution of VHF backscatter turbulence echoes, ignoring echoes with azimuths $< 0°$ and $> 20°$, whose altitudes are anomalous (Ivarsen et al., 2023). Remarkably, throughout the 40-minute interval, the peak altitude from the two datasets match, and exhibit a very similar downward trend (Figure 1d, f), with the peak of the turbulent layer (as well as the peak impact altitude) decreasing at a rate of around 5 m/s, or 13 km through the 40-minute interval. This sinking of the ionosphere is caused by the onset of a moderate magnetospheric substorm (Newell and Gjerloev, 2011b), evidenced by the SuperMAG electrojet (SME) index, (Newell and Gjerloev, 2011a), shown in Figure 1e).

The event in Figure 1 featured a rare direct conjunction, of which there are few [and we direct the reader towards a notable such direct conjunction in Ivarsen et al. (2025a)]. Figure 2 shows an indirect conjunction, where Arase's ionospheric footprint was situated a few hundred kilometers west of ICEBEAR's field-of-view, akin to Ivarsen et al. (2025c), and following that study, we shift the Arase observations backward in time, finding that ICEBEAR observes the same dynamics 3 minutes and 20 seconds after Arase. However, whereas the previous conjunction event took place when Arase was situated in the generator region of the auroral magnetosphere (some 20° raised from magnetospheric equator), the conjunction event in Figure 2 took place when Arase was situated *inside the radiation belts*, $< 5°$ from magnetospheric equator, some five Earth radii distant from the E-region. Such conjugate data contains both the driver (plasma wave interactions with electrons, observed by Arase) and the resulting turbulence (FB waves observed by ICEBEAR), and the two can evolve in lockstep (Ivarsen et al., 2025a).

We observe such lockstep evolution in Figure 2, with a tight correlation, albeit with a 3 minute 20 second lag. To demonstrate this lockstep evolution, we have implemented a constrained multivariable linear regression, to model the occurrence rate of ionospheric VHF radar echoes, $n(t)$, as a function of magnetospheric wave power inside certain frequency bands, building on Ivarsen et al. (2025a),

$$\hat{n}(t) = \sum_{i=1}^{4} \left[\beta_{2i-1} + \beta_{2i} \log_{10}(x_i(t - \tau_i))\right], \tag{47}$$

https://doi.org/10.5194/egusphere-2026-2345
Preprint. Discussion started: 21 May 2026

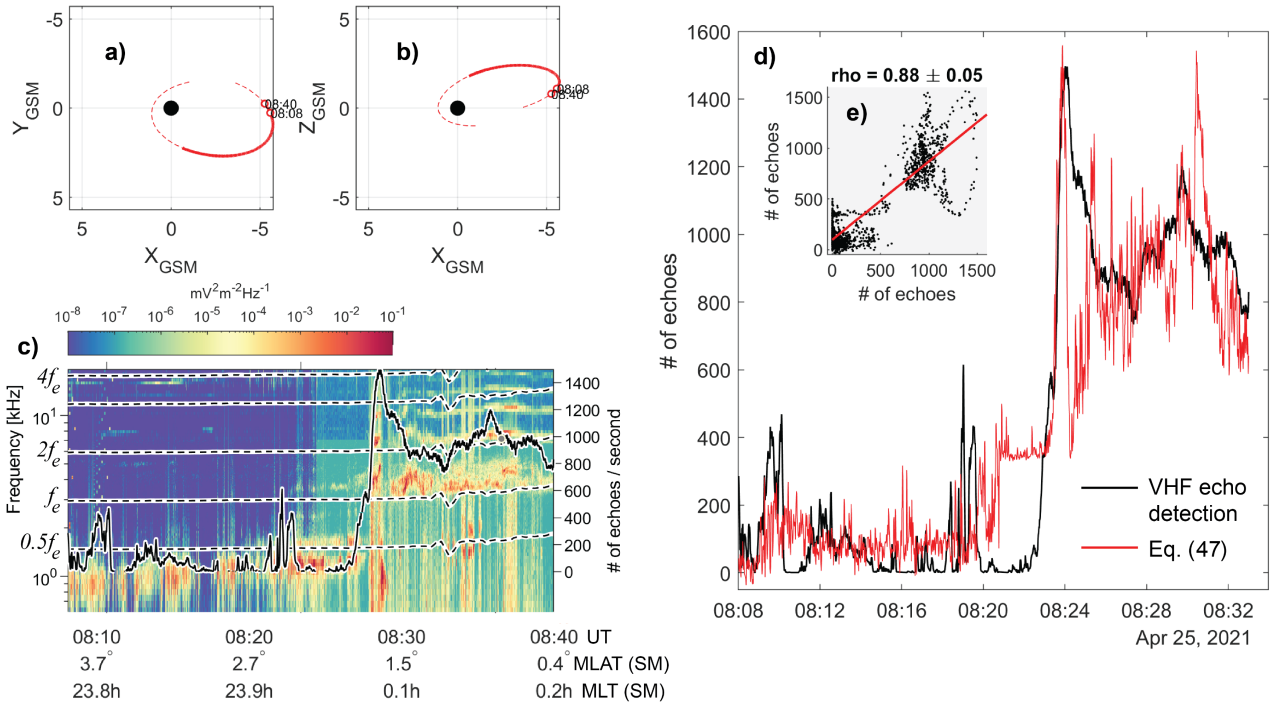

Figure 2. Panels a) and b) show Arase's position in the magnetosphere during the conjunction, in units of Earth radii. **Panel c)** shows the electric field wave power measured by the PWE instrument (Kasahara et al., 2018c), as a spectrogram, with frequency along the y-axis and time along the x-axis. Multiples of the local electron cyclotron frequency f_e [measured using the MGF instrument (Matsuoka et al., 2018)] is shown in dashed black lines, identifying four frequency bands. The rate of observed VHF echoes is superposed in black, and the Arase-data is shifted 3 m 20 s backwards in time. **Panel d)** shows the multivariable linear regression model (Eq. 47) in red, compared with the observed echo detection rate in black; the two timeseries have a resolution of 1 s and are highly correlated, with a linear regression analysis shown in the inset **Panel e)** (Pearson correlation coefficient ρ is indicated at 0.88 ± 0.05, with error margin given by the 95% confidence interval of the linear regression, or 3σ). The model Eq. (47) defines the response variable as the radar echo rate and the predictor variables as the base-10 logarithms of the wave power integrated across the four distinct frequency bands on display in Panel c); see Figure 4 in the Appendix for details of the frequency-dependent power, as well as the geospatial locations of the instruments.

https://doi.org/10.5194/egusphere-2026-2345
Preprint. Discussion started: 21 May 2026

where β_{2i-1} and β_{2i} are intercept and slope respectively, for the four frequency bands, with x_i being the magnetospheric wave power (root-mean-square) for the i^{th} frequency band on display in Figure 2c). As we detail in Appendix A, highest correlation is found in the $f_e < f < 2f_e$ band, characteristic of electrostatic cyclotron harmonic waves. τ_i is an additional lag (deviating from the stated 3 m 20 s); and we observe that the first frequency interval, which corresponds to the lower-band chorus waves with $0.1f_e < f < 0.5f_e$, is shifted an additional 20 s backwards, whereas the three other frequency bands are best correlated at the stated lag of 3 m 20 s. To estimate the eight β-parameters in Eq. (47), we apply a constrained optimization routine (MATLAB's `fmincon` algorithm), which minimizes the mean squared error between the observed n and predicted $\hat{n}$. The parameter space is strictly bounded to enforce non-negativity across all slopes and intercepts.

The analysis reveals a striking Pearson correlation coefficient between n and $\hat{n}$ of $\rho = 0.88 \pm 0.05$. This result echoes several recent investigations that all demonstrate that auroral turbulence in the E-region can be used as proxy observations for magnetospheric wave processes, and vice versa (Ivarsen et al., 2024a; Shen et al., 2024; Ivarsen et al., 2025a, b). This proxy status is explained by the theoretical foundation built in Sections 1 and 2: any excess driving electric field that surpasses ~ 20 mV/m is near-instantly counteracted by the saturation of the Farley-Buneman instability, forcing radar observations of the latter to evolve in close accordance with the magnetospheric driving signal, thereby leading to directly driven small-scale plasma turbulence without hysteresis or inertia.

3.1 Statistical aggregate

Conjunctions like those shown in Figures 1 and 2 are rare. However, a considerable database of observations have been amassed for both ICEBEAR and Arase, and we can discern clear trends by comparing observations that were made within the same region of geospace; i.e., the nightside auroral oval, during a wide variety of geomagnetic conditions. For the four years between 2020 and 2023 inclusive, we have collected 1.2 million one-second intervals of VHF echo detection, corresponding to the identification of a total of 272 million echoes, and we compare this database with the concurrent observation by Arase of some 530,000 electric wave-spectra, observed when Arase was within 5° of magnetospheric equator, on nights during which ICEBEAR was operational.

The wide variety of conditions that the foregoing datasets cover allows us to statistically describe the energy transfer of ionosphere-magnetosphere coupling during such observations of intense auroral plasma turbulence. In Figure 3 we show median values of the VHF radar echo detection rate n and the total integrated wave power ΔE, for 15 geomagnetic activity bins [see the Appendix B in Ivarsen et al. (2025a) for details about this dataset]. In Figure 3a), we observe a distinct elbow in the curve at an auroral electrojet value of around 150 nT, below which the echo detection rate is flat (meteor trail echoes (Oppenheim et al., 2003; Hussey et al., 2000; Ivarsen et al., 2023)) For bins above this elbow, the bin-median echo detection rate is near-perfectly correlated with the auroral electrojets ($\rho = 0.99$), and at the same threshold, we observe that the wave power locks into a consistent scaling with the electrojet index $\rho = 0.95$). We label this elbow with the critical wavepower ΔE_c. When the magnetospheric wave power exceeds this threshold, the two quantities exhibit a similar response to enhancements in the electrojets, facilitating the linear ($\beta = 0.98 \pm 0.09$) relationship shown in Figure 3c).

https://doi.org/10.5194/egusphere-2026-2345
Preprint. Discussion started: 21 May 2026

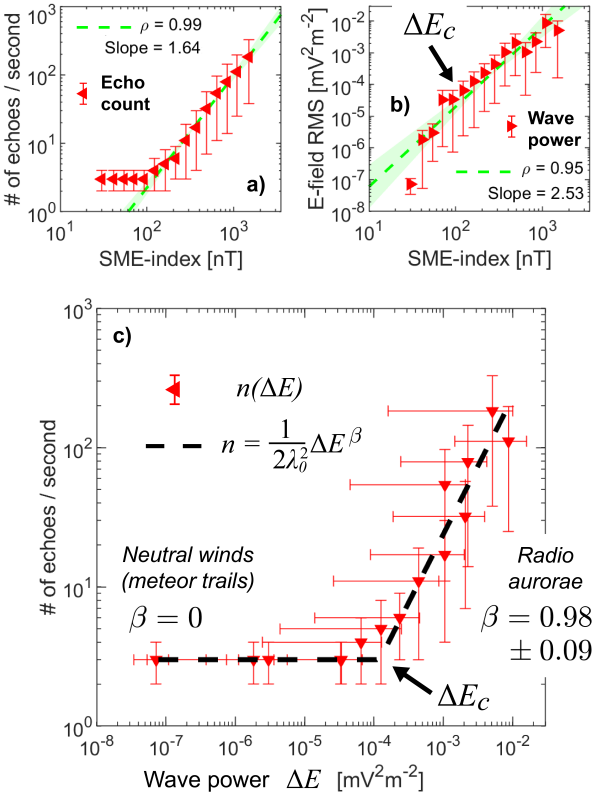

Figure 3. Panel a) aggregates the ICEBEAR echo detection rate, for some 1.2 million one-second intervals (containing a total of 272 million echoes), while **Panel b)** aggregates Arase-observed wave power (integrated wave spectra for frequencies $f > 0.1 f_e$, f_e being the electron cyclotron frequency) for some 530,000 one-second wave spectra, measured using the Plasma Wave Experiment on board Arase (Kasahara et al., 2018c), using measurements from when the satellites was within 5° off magnetospheric equator, and during magnetic local times (Baker and Wing, 1989) between 22h and 06h, with data collected on days when the radar was operational (between January 2020 and June 2023). In both panels e) and f), red triangles represent the median value inside 15 logarithmically spaced geomagnetic activity bins (using the SME-index, (Newell and Gjerloev, 2011a) or auroral electrojet index). Vertical errorbars denote upper/lower quartile distributions. Linear fits are indicated, by non-linear least squares minimization of the root-mean-square error. **Panel c)** shows the same 15 bins in a scatterplot, with a black dashed line denoting $n \propto \Delta E^\beta$ (see Eq. 52), with $\beta = 0$ when $\Delta E < \Delta E_c$ and $\beta = 0.98 \pm 0.09$ otherwise, determined through non-linear least squares minimization, where $\Delta E_c \sim 10^{-4}$ mV^{2}m^{-2} represents the critical wave power. Statistical error margin is posted showing 95-percent confidence intervals for β (3-sigma), using a Monte Carlo-based bootstrapping routine with 500 iterations and a randomized data selection for each iteration.

https://doi.org/10.5194/egusphere-2026-2345
Preprint. Discussion started: 21 May 2026

4 Discussion

Penetrating electric fields produced by Hall currents and corresponding energetic particle precipitation carry Alfvén waves to the upper atmosphere, the ionospheric E-region. Here, impedance matching and its effect on Joule heating (as well as turbulent heating), allow for a self-organized criticality to emerge in the interplay between the driver and the immediately responding FB turbulence. This immediacy, or ephemeral quality, is accompanied by a reduction in electric field (inside the turbulent regions) to the ion acoustic speed, which limits the amplitude of FB waves – but their numbers. Any response beyond the saturation to the ion sound speed is immediately counter-acted by polarization electric fields, whose multitude we have analyzed in the present study. In a companion paper [CITE COMPOSITE SPECTRA PAPER HERE], we provide evidence for a persistent kinetic ALfvén signature in composite radar–GNSS measurements of auroral plasma turbulence.

In the present paper, the statistical aggregates in Figure 3 clearly identifies a linear, statistical scaling between the packing of FB waves and the driving wave power observed near the radiation belts. The specific physical mechanism enforcing this linear scaling between the driver and the proliferation of FB turbulence ($\beta \approx 1$) can be derived from the non-linear evolution of finite plasma structures. Following St.-Maurice and Hamza (2001), we consider that an initial density perturbation evolves as a finite structure that generates internal polarization electric fields. These fields oppose the driver, effectively reducing the internal electric field until the drifts barely exceed the threshold condition (C_s). (Oppenheim and Dimant, 2013) This feedback mechanism explains the pervasive observation of phase velocities saturated near the ion-acoustic speed (Foster and Erickson, 2000; Oppenheim and Dimant, 2013). Crucially, the aggregate intensity of the turbulence is determined by the density of these structures within the unstable volume. We posit a space-time equivalence where the number of active scatterers, n, is proportional to the linear growth rate γ_{lin}. (Drexler et al., 2002) Since the fluid growth rate scales as $\gamma_{\text{lin}} \propto (V_d^2 - C_s^2)$, and the drift velocity V_d is proportional to the external electric field E, the strongly driven regime ($V_d^2 \gg C_s^2$) yields a scatterer density $n \propto E^2$ (see Section 2.1.3). The linear response is therefore a direct consequence of the instability actively populating the volume in proportion to the available free energy.

A rigorous application of renormalization group theory (Wilson, 1971) completes the foregoing phenomenological description (see Section 2.1). By reconstructing an action in the path-integral formulation, working backwards from the dispersion relation Eq. (1), we apply a spacetime rescaling ($x' \to b^{-1}x$), after which the inertial operator responsible for acceleration becomes irrelevant, decaying as b^{-2} at macroscopic scales. Consequently, the system flows inevitably toward a stable, *overdamped* fixed point (dynamic exponent $z = 2$).

The overdamped equations of motion define an effective field theory with an inferred cutoff (correlation scale) given by (see Section 2.1.4):

$$L_c = \frac{2\sqrt{2}\pi D_{\text{eff}}}{V_d - C_s}, \tag{48}$$

where V_d is the saturated drift. L_c features a divergence at the threshold (C_s), characteristic of a continuous phase transition (Hohenberg and Halperin, 1977), but the excess drift saturates at around $1.1C_s$ inside the turbulent regions (Hamza and St-Maurice, 1993; Oppenheim and Dimant, 2013), keeping Eq. (48) finite.

https://doi.org/10.5194/egusphere-2026-2345
Preprint. Discussion started: 21 May 2026

The turbulent amplitude field $\psi = \delta N_e/N_{e,0}$ is governed by an effective transport equation. Here, $V_d > C_s$ triggers turbulence growth via negative diffusion. (Ashinsky, 1988) The net stability condition decomposes into a driving term (source) and a saturation term (sink) (Eq. 26):

$$D_{\parallel} \approx \gamma_{\text{eff}}^{-1} \left[(C_s^2 - V_{d0}^2) + 2\tilde{\alpha} V_{d0}^2 |\psi|^2 \right]. \tag{49}$$

Marginal stability implies a balance where the net diffusion vanishes ($D_{\parallel} \to 0$), meaning the anomalous saturation term must exactly cancel the unstable driver. Physically, this corresponds to an anomalous electric field,

$$E_{\text{anom}} \approx (V_{d0} - C_s)B, \tag{50}$$

that acts as a macroscopic drag force. This drag underpins the resistive non-linear currents (Dimant et al., 2021) and wave-heating (St.-Maurice and Chau, 2016) observed *in-situ* and in kinetic simulations. Figure 3c) offers clues as to how this drag manifests in the dynamics. The observed linear relationship $n \propto \Delta E$ implies that the *number density of turbulent waves* obeys Ohm's law as a constant-resistance load. This validates the definition of an anomalous resistivity $\eta \equiv E_{anom}/J$, which scales as $\eta \approx (B/n_e e)(1 - C_s/V_{d0})$ given the free energy source $J = n_e e V_{d0}$. To close the macroscopic transport model, we consider the generalized Einstein relation for non-equilibrium steady states, (Harada and Sasa, 2005; Loi et al., 2011) $D_{\text{eff}} \approx \mu k_B T_{\text{eff}}$, where k_B is the Boltzmann constant. Since the turbulent fluctuations are spectrally limited by the thermal saturation scale (C_s), we adopt $T_{\text{eff}} \approx T_e$ and obtain $D_{\text{eff}} \approx T_e/n_e e^2 \eta$. For the density fluctuations ψ, this yields the effective diffusion coefficient,

$$D_{\parallel} = \frac{T_e}{eB} \left(1 - \frac{C_s}{V_{d0}} \right)^{-1} \xrightarrow{V_{d0} \gg C_s} \frac{T_e}{eB}. \tag{51}$$

Thus, the friction generated by the electron slip stream is identified as the anomalous transport coefficient '*Bohm*', (Kaufman, 1990; Treumann and Baumjohann, 1997; Burch et al., 2016; Braginskii, 1965; Ott and Bonitz, 2011) a phenomenological staple in plasma studies.

We note that while equating the effective noise temperature to the ambient electron temperature provides a mathematically elegant closure to recover macroscopic Bohm diffusion, it should be treated as an idealized phenomenological parameterization rather than a rigorously derived kinetic certainty.

We can use Eq. (51) to demarcate the field theory's area of validity. We write $L_c \approx (2\sqrt{2}\pi/0.1C_s)(T_e/eB)$. With $T_e \sim 0.1$ eV and $B \sim 50{,}000$ nT, we obtain $L_c \sim 350$ m. For scales $L \lesssim 350$ m, the effective field theory is valid, and the stochastic sum total of polarization electric fields renormalizes into Bohm resistivity in the electron slip stream, in the Hall currents. Because the electron fluid is in a critical state of thermal saturation, the anomalous response field E_{anom} is near-instantly generated to maintain marginal stability, forcing the electron transport to strictly track the spatio-temporal structure of the magnetospheric driver (V_{d0}).

We next follow our effective field theory to its logical conclusion. In the macroscopic limit, the phase dynamics of the overdamped turbulent waves reduce to the Adler equation for synchronization phenomena (Adler, 1946). Consequently, we recover the observed linear response (Eq. 42),

$$n \propto \frac{1}{2\lambda_0^2} \Delta E, \tag{52}$$

https://doi.org/10.5194/egusphere-2026-2345
Preprint. Discussion started: 21 May 2026

where λ_0 is the effective damping at the dissipative fixed point, which retains the Bohm scaling, $\lambda_0 = D_{\text{eff}}k^2 = (4\pi^2/9)(T_e/eB)$ at the radar wavelength. This response matches the empirical result (Figure 3c), allowing us to identify the system's behavior with the current-voltage ("I-V") characteristics of an overdamped Josephson junction. (Stewart, 1968; Ambegaokar and Halperin, 1969; Wiesenfeld et al., 1996) In this analogy, the transition from a static 'locked' state to a phase-slipping 'running' state corresponds to the onset of the electron slip stream ($V_{d0} > C_s$). Crucially, the response in Figure 3c) exhibits the signature of a *noise-broadened bifurcation* (Ambegaokar and Halperin, 1969; Danner et al., 2021), confirming that the onset of the 'running' state, $V_d > C_s$, is a critical point created by the renormalized *noise* of the ensemble's saturation electric fields.

The Adler-Ohmic bifurcation at ΔE_c denotes a characteristic behaviour in physical systems where oscillating constituents create a voltage drop against an effective tilted washboard potential, one that facilitates a 'running', or phase slipping, state, following a threshold of disorder. (Ambegaokar and Halperin, 1969) That we are able to observe this macroscopic description in the particular magnetosphere-ionosphere coupling created by Farley-Buneman waves, implies that the constituents of *that* system likewise lock or slip against an effective tilted washboard potential. Subsequently, the magnetosphere-ionosphere coupling near intense diffuse aurorae is kept in a critical state sustained by efficient, turbulent energy dissipation, and its macroscopic description is ultimately governed by 'Model A' universal dynamics, (Hohenberg and Halperin, 1977) a class of purely dissipative systems.

However, we highlight that the measurements that enabled this insight span *multiple systems* in geospace; the locked state in Figure 3c) is represented by meteor trail echoes, (Ivarsen et al., 2023) created when meteors burn up in the atmosphere. Friction creates intense, short-lived plasma turbulence (Oppenheim et al., 2003), and the backscatter echoes from this turbulence act as tracers for the neutral winds(Hall et al., 1997; Hussey et al., 2000; Kumar, 2007). ICEBEAR is capable of detecting and distinguishing meteor trail echoes (Ivarsen et al., 2023), but When parameterized by observed magnetospheric wavepower, the meteor trail turbulence shows no response, and therefore functions as a latent tracer for the turbulence within the system. The association of Adler-Ohmic bifurcation at ΔE_c is therefore a characterization of *the auroral ionosphere as a system,* and specifically its turbulent response to external driving.

While the foregoing interpretation must be substantiated and elucidated by observations in closer detail, the immediate implications of our results can aid ongoing efforts. When saturation feedback effectively governs the system under study, the turbulent regions evolve without hysteresis, providing an explanation for observations of directly driven auroral plasma turbulence with zero or near-zero lag, (Shen et al., 2024; Ivarsen et al., 2025a; Brindley et al., 2025) as well as justification for the omission of hysteresis in global turbulence models (Wiltberger et al., 2017a).

Our field theory, however, represented by the derivation of complete, closed-form macroscopic transport relations (culminating in Eq. 51), offer a useful tool. It implies that, in two-stream plasmas, whenever the driving field attempts to push the drift velocity beyond the sound barrier, the system automatically generates Bohm resistivity to clamp the flow to the ion acoustic speed, providing strong justification for the application of Bohm diffusion in numerical models of the auroral ionosphere. The expenditure of Bohm diffusion is accomplished through saturation electric fields, in a stochastic ensemble. *The FB turbulence generates exactly enough noise, or effective temperature ($T_{eff} \approx T_e$) to assemble a thermal diffusion process at the*

https://doi.org/10.5194/egusphere-2026-2345
Preprint. Discussion started: 21 May 2026

acoustic scale. This provides a useful constitutive relation for modeling anomalous currents and heating in global ionospheric simulations.

Lastly, we stress that, while interpreting the observed linear proliferation of turbulence in the auroral ionosphere system (Figure 3c) as an Adler-Ohmic bifurcation provides an exceptionally well-fitting statistical envelope for large-scale modeling, it remains highly uncertain whether the plasma structures genuinely achieve the concerted macroscopic phase-locking characteristic of microelectrical devices.

5 Conclusion

In this investigation, we have pinpointed a clear emergent regime in auroral plasma turbulence, which we posit is produced by Alfvénic impedence matching establishing a dynamic equilibrium, or criticality. We explore the core mechanism in this emergent effect, namely the statistical effect of exciting thousands or millions of FB waves inside a limited volume inside the auroral electrojets.

We explore this mechanism in terms of a renormalization group (RG) theoretical treatment of Farley-Buneman turbulence, as well as a massive dataset of observations by radar (final energy expenditure) and spacecraft (driver). The dataset shows clearly that the driver and expenditure produces a statistical "I-V" curve that is the exact expectation from an interconnected array of Josephson junctions. This central result is interpreted in one of two ways:

(1, strong) First, we treat the theoretical possibility that the striking emergent behaviour that we have described in Figure 3 leads directly to space weather changes through concerted fluctuations around locked frequencies akin to Josephson synchronization in superconductivity theory. In other words, this is the interpretation of the curve in Figure 3c) that it *is* an I-V curve; and this interpretation follows directly from the renormalization performed in Section 2.1: switching between the quiescent and turbulent states necessitates that the space weather system is subject to a tilted washboard potential (Ambegaokar and Halperin, 1969), opening up completely novel strands of theoretical investigation of auroral plasma turbulence. Although justified by theory, and supported by statistical evidence, there is not sufficient reason to claim that the parcels of turbulent plasma around aurorae function as interconnected Josephson junctions.

(2, weak) The second interpretation is practical, and concerns space weather modeling. Numerical, fluid solutions of the magnetohydrodynamics around Earth are unable to resolve scales smaller than a certain boundary, dictated largely by reasons of computational cost, referred to as a grid-cell. Below this scale, simulations must take both kinetic and fluid eventualities into account, and are accordingly *very* computationally costly, the so-called hybrid fluid-kinetic solutions to the Farley-Buneman instability (Oppenheim et al., 1995; Wiltberger et al., 2017b; Dimant and Sudan, 1995; Dimant et al., 2021). This is an instance where space weather shares a known vulnerability with conventional hydrodynamic weather modeling of Earth's atmosphere: the nature and magnitude of the turbulent cascade remains unknown in space weather modeling for scales smaller than around 50-100 km, and must be evaluated using expensive numerical simulations.

In terrestrial climate science, resolving this grid-cell vulnerability has historically relied on parameterizing the sub-grid cascade as effective diffusion (Smagorinsky, 1963), and more recently, through stochastic parameterization that treats unresolved

https://doi.org/10.5194/egusphere-2026-2345
Preprint. Discussion started: 21 May 2026

convective scales as noise (Palmer, 2012; Berner et al., 2017). In ionospheric physics, turbulence parameterization through eddy diffusion has likewise been frequently applied in global models (Roble et al., 1988; Wu et al., 2017; Vaishnav et al., 2021), and stochastic parameterization has been applied in magnetospheric modeling (Watt et al., 2022). By formalizing Farley-Buneman micro-fields as a stochastic variable, our application of RG theory (Section 2.1) effectively imports this probabilistic Earth-system framework into high-latitude electrodynamics, offering explicitly renormalized coefficients in three dimensions that elucidate the transport of momentum and energy "sub-grid." We emphasize this last point; the three dimensions entertained by our diffusion tensor mean that, unlike scalar eddy diffusion, our transport coefficients retain the anisotropic structure of the instability, and it is determined by specific saturation physics rather than prescribed according to empiri.

Regardless of whether one subscribes to ***(1)*** or ***(2)*** above, we maintain that, in presenting these results, we have shed crucial light on the potential for a specific novel process (described by non-linear synchronization theory). This prospect must be further elucidated, but, at present, we suffice to provide the foundation for a concrete and productive application of RG theory for the purpose of space weather modeling. We thereby conclude with the abridged summary that kinetic processes in auroral plasma turbulence may act in apparent concert to produce a distinct synchronization phenomena in the auroral ionosphere, one that is only observable in statistical aggregates, and is otherwise confined to the physics of microelectrical, superconductive devices.

https://doi.org/10.5194/egusphere-2026-2345
Preprint. Discussion started: 21 May 2026

Appendix A: Cross-correlation and multivariable regression methodology

This appendix details the statistical framework and lag analysis utilized to correlate magnetospheric wave power with the occurrence rate of ionospheric Farley-Buneman turbulence, supporting the multivariable linear regression model presented in Eq. (47).

To account for the broadband nature of the magnetospheric 'driving signal', the electric field wave spectra observed by the Arase spacecraft are partitioned into discrete frequency bands. These bands are defined relative to the local electron cyclotron frequency, f_e, allowing for the isolation of specific wave modes, such as lower-band chorus waves ($0.1f_e < f < 0.5f_e$) and electrostatic cyclotron harmonic waves ($f_e < f < 2f_e$), where we follow the approach of Ivarsen et al. (2025a).

Because wave-particle interactions, pitch-angle scattering, and subsequent precipitation of electrons along magnetic field lines introduce complex, frequency-dependent delays that adhere to a host of local physical processes, a rigorous cross-correlation analysis is necessary to map the driving signal to the resulting ionospheric response. A baseline macroscopic propagation lag is established between the inner magnetosphere and the E-region—determined in this event to be 3 m 20 s. To refine this mapping, a sliding-window cross-correlation is applied independently across the spectral bands (as detailed in Figure 4e) to identify specific temporal deviations, τ_i, from the baseline lag (see Eq. 47).

With the optimal frequency-dependent lags established, the radar echo detection rate, $\hat{n}(t)$, is modeled as a linear combination of the lagged, logarithmically scaled wave powers within each frequency regime. A constrained optimization algorithm minimizes the mean squared error to extract the domain-specific slopes (β_{2i}) and intercepts (β_{2i-1}). The parameter space is strictly bounded to enforce non-negativity across all coefficients, reflecting the assumption that the high-latitude Farley-Buneman instability acts as a strictly driven, non-hysteretic dissipative sink for the external free energy. Finally, this temporal analysis inherently relies on an assumption of spatial coherence across the longitudinal and latitudinal separation between the radar's observational volume and the mapped ionospheric footprint of the spacecraft (Figure 4g).

We note with interest how the four red signals in Figure 4a–d) show distinct and, in places, strong correlation with the black signal, echoing Ivarsen et al. (2025a).

https://doi.org/10.5194/egusphere-2026-2345
Preprint. Discussion started: 21 May 2026

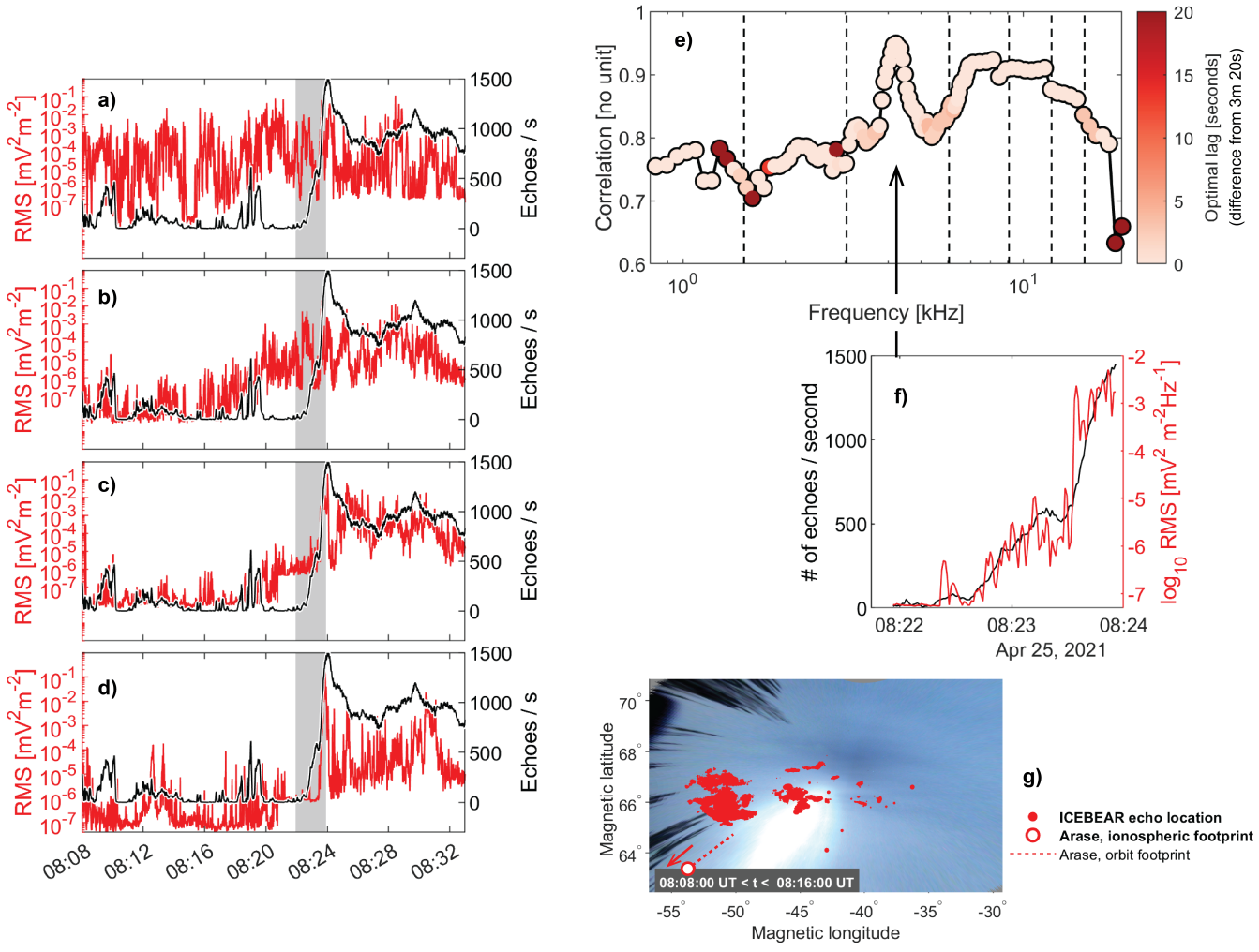

Figure 4. Additional information underlying the analysis in Figure 2 and Eq. (47). **Panels a–d)** show, with solid red line, integrated power inside the four frequency bands shown in Figure 2c, with the VHF echo detection rate superposed (black). **Panel e)** shows a cross-correlation analysis applied to each individual frequency, with a white-red colorscale denoting optimal lag (deviation from the stated 3 m 20 s). The point of highest correlation is the explosive onset of activity, which is shown in **Panel f**). **Panel g)** shows the relative distances between observed VHF echo locations and the ionospheric footprint of Arase, superposed on a TREx RGB image that exhibits considerable light pollution from the moon (the white blob).

https://doi.org/10.5194/egusphere-2026-2345
Preprint. Discussion started: 21 May 2026

Appendix B: Phenomenological derivation of the linear scaling law

In this appendix, we shall present a qualitative explanation, as an alternative to our RG theory application, as to why the statistical aggregate of FB turbulence exhibits a linear scaling against magnetospheric wave power.

The mathematical substitution of the deterministic mode-coupling term ($\psi\nabla\psi$) with a stochastic noise term ($\delta\mathbf{v}$) constitutes random phase approximation, which formally lumps the turbulent cascade into a diffusion term. Methodologically, this allows the macroscopic scale separation to be achieved entirely through the temporal coarse-graining of uncorrelated phase histories, rather than relying on spatial momentum-shell integration. By discarding the phase correlations required for three-wave interactions, this approach explicitly neglects the dynamic flux of energy across scales and treats the plasma as an ensemble of turbulent waves rather than a structured fluid capable of forming shocklets. This departure from a fluid description is validated by the two-stream origin of the instability: saturation is dominated by local electrostatic feedback (where polarization fields clamp the local drift to C_s), a notion that is firmly supported by Figure 3b, as well as the state of electrojet turbulence research [see, e.g., Foster and Erickson (2000); Oppenheim and Dimant (2013); Koustov et al. (2005); Chau and St.-Maurice (2016)].

A phenomenological argument based on the foregoing recovers the central result (Eq. 42), by way of adiabatic elimination. On time scales longer than the initial growth time, the unstable structures will lose amplitude after zero growth is approached: Drexler et al. (2002) showed that the eigenfrequency is a weak function of space (altitude), which forces the introduction of steadily increasing parallel electric fields inside unstable structures. Such fields short-circuit the internal, perpendicular fields by passing parallel currents. (Oppenheim and Dimant, 2013) This, incidentally, gives the wave energy to electrons which in turn give it to the gas through inelastic collisions. (St-Maurice and Goodwin, 2021)

Assume, then, that inside an unstable volume, the faster the individual structures grow, the more of them there are. This introduces an equivalence between time and space: shorter growth times mean more structures. *The number of structures in an unstable volume is therefore proportional to the linear growth rate.* Using fluid theory approximation as a guide this means that the number of structures inside the unstable volume is given by,

$$n \propto a\frac{\Psi}{1+\Psi}\frac{k^2}{\nu_i}(V_d^2 - C_s^2), \tag{53}$$

where a is a constant, ν_i the ion-neutral collision frequency, and V_d is the relative ion-electron drift, very close to E/B at 100 km altitude. Therefore, when V_d^2 is well above C_s^2, the number of VHF radar backscatter targets becomes essentially proportional to the electric field squared, E^2. With a dominance of the 500 to 600 m/s threshold speed observed at 100 km, E/B has to be exceeding 1500 m/s (see Figure 1 in St-Maurice et al. (2023), and the near proportionality to E^2 is justified.

https://doi.org/10.5194/egusphere-2026-2345
Preprint. Discussion started: 21 May 2026

Author contributions. MFI conceived of the study, performed data analysis, and wrote the manuscript. GCH operated the radar, provided data handling, and conceived of the radar. DRT & YM provided feedback on the manuscript. YM, AS, & SY operated the Arase satellite and provided data handling.

Competing interests. At least one of the (co-)authors is a member of the editorial board of Annales Geophysicae.

Data availability Science data of the ERG (Arase) satellite were obtained from the ERG Science Center operated by ISAS/JAXA and ISEE/Nagoya University (https://ergsc.isee.nagoya-u.ac.jp/index.shtml.en. This includes Lv.3 HEP (DOI 10.34515/DATA.ERG-01002) version 01_01, Lv.3 MEP-e (DOI 10.34515/DATA.ERG-02003) version 01_01, Lv.2 LEP-e (DOI 10.34515/DATA.ERG-05000) version 04_01, Lv.2 PWE/OFA (DOI 10.34515/DATA.ERG-08000), and Lv.2 MGF (DOI 10.34515/DATA.ERG-06001) version 04_04. SuperMAG data can be accessed at https://supermag.jhuapl.edu/mag/.ICEBEAR 3D echo data for 2020, 2021 is published with DOI 10.5281/zenodo.7509022.

Acknowledgements. This work is supported in part by the European Space Agency's Living Planet Grant No. 1000012348 and by the Research Council of Norway (RCN) Grant No. 324859. We acknowledge the support of the Canadian Space Agency (CSA) [20SUGOICEB], the Canada Foundation for Innovation (CFI) John R. Evans Leaders Fund [32117], the Natural Science and Engineering Research Council (NSERC), the Discovery grants program [RGPIN-2019-19135], the Digital Research Alliance of Canada [RRG-4802].DRT is supported through UK Natural Environment Research Council DRIIVE [NE/W003368/1] and FINESSE [NE/W003147/1] grants. Google's Gemini 3.0 Pro has been used to assist mathematical formalism. MFI is grateful to J.P. St-Maurice, M. Oppenheim, D. Knudson, J. Park, and R. Horne for stimulating discussions during the preparation of this manuscript.

https://doi.org/10.5194/egusphere-2026-2345
Preprint. Discussion started: 21 May 2026

References

Adler, R.: A Study of Locking Phenomena in Oscillators, Proceedings of the IRE, 34, 351–357, https://doi.org/10.1109/JRPROC.1946.229930, 1946.

Ambegaokar, V. and Halperin, B. I.: Voltage Due to Thermal Noise in the Dc Josephson Effect, Physical Review Letters, 22, 1364–1366, https://doi.org/10.1103/PhysRevLett.22.1364, 1969.

Andersen, H. C.: Functional and Graphical Methods for Classical Statistical Dynamics. I. A Formulation of the Martin–Siggia–Rose Method, Journal of Mathematical Physics, 41, 1979–2020, https://doi.org/10.1063/1.533223, 2000.

Ashinsky, G. I.: Nonlinear Analysis of Hydrodynamic Instability in Laminar Flames—I. Derivation of Basic Equations, in: Dynamics of Curved Fronts, pp. 459–488, Academic Press, https://doi.org/10.1016/B978-0-08-092523-3.50048-4, 1988.

Bahcivan, H., Hysell, D. L., Lummerzheim, D., Larsen, M. F., and Pfaff, R. F.: Observations of Colocated Optical and Radar Aurora, Journal of Geophysical Research: Space Physics, 111, https://doi.org/10.1029/2006JA011923, 2006.

Baker, K. B. and Wing, S.: A New Magnetic Coordinate System for Conjugate Studies at High Latitudes, Journal of Geophysical Research: Space Physics, 94, 9139–9143, https://doi.org/10.1029/JA094iA07p09139, 1989.

Berner, J., Achatz, U., Batté, L., Bengtsson, L., de la Cámara, A., Christensen, H. M., Colangeli, M., Coleman, D. R. B., Crommelin, D., Dolaptchiev, S. I., Franzke, C. L. E., Friederichs, P., Imkeller, P., Järvinen, H., Juricke, S., Kitsios, V., Lott, F., Lucarini, V., Mahajan, S., Palmer, T. N., Penland, C., Sakradzija, M., von Storch, J.-S., Weisheimer, A., Weniger, M., Williams, P. D., and Yano, J.-I.: Stochastic Parameterization: Toward a New View of Weather and Climate Models, Bulletin of the American Meteorological Society, 98, 565–588, https://doi.org/10.1175/BAMS-D-15-00268.1, 2017.

Bonicelli, A., Dappiaggi, C., and Drago, N.: An Algebraic Correspondence Between Stochastic Differential Equations and the Martin–Siggia–Rose Formalism, Annales Henri Poincaré, https://doi.org/10.1007/s00023-025-01571-1, 2025.

Braginskii, S. I.: Transport Processes in a Plasma, Reviews of Plasma Physics, 1, 205, 1965.

Brindley, N., Madhanakumar, M., Spicher, A., Whiter, D., Oksavik, K., and Ogawa, Y.: Intense Dynamic Optical Auroral Sub-Structure as a Proxy for Ionospheric Density Irregularities, Journal of Geophysical Research: Space Physics, 130, e2025JA033 999, https://doi.org/10.1029/2025JA033999, 2025.

Buneman, O.: Excitation of Field Aligned Sound Waves by Electron Streams, Physical Review Letters, 10, 285–287, https://doi.org/10.1103/PhysRevLett.10.285, 1963.

Burch, J. L., Torbert, R. B., Phan, T. D., Chen, L.-J., Moore, T. E., Ergun, R. E., Eastwood, J. P., Gershman, D. J., Cassak, P. A., Argall, M. R., Wang, S., Hesse, M., Pollock, C. J., Giles, B. L., Nakamura, R., Mauk, B. H., Fuselier, S. A., Russell, C. T., Strangeway, R. J., Drake, J. F., Shay, M. A., Khotyaintsev, Yu. V., Lindqvist, P.-A., Marklund, G., Wilder, F. D., Young, D. T., Torkar, K., Goldstein, J., Dorelli, J. C., Avanov, L. A., Oka, M., Baker, D. N., Jaynes, A. N., Goodrich, K. A., Cohen, I. J., Turner, D. L., Fennell, J. F., Blake, J. B., Clemmons, J., Goldman, M., Newman, D., Petrinec, S. M., Trattner, K. J., Lavraud, B., Reiff, P. H., Baumjohann, W., Magnes, W., Steller, M., Lewis, W., Saito, Y., Coffey, V., and Chandler, M.: Electron-Scale Measurements of Magnetic Reconnection in Space, Science, 352, aaf2939, https://doi.org/10.1126/science.aaf2939, 2016.

Chau, J. L. and St.-Maurice, J.-P.: Unusual 5 m E Region Field-Aligned Irregularities Observed from Northern Germany during the Magnetic Storm of 17 March 2015, Journal of Geophysical Research: Space Physics, 121, 10,316–10,340, https://doi.org/10.1002/2016JA023104, 2016.

https://doi.org/10.5194/egusphere-2026-2345
Preprint. Discussion started: 21 May 2026

Danner, L., Padurariu, C., Ankerhold, J., and Kubala, B.: Injection Locking and Synchronization in Josephson Photonics Devices, Physical Review B, 104, 054 517, https://doi.org/10.1103/PhysRevB.104.054517, 2021.

Dimant, Y. S.: Deriving Improved Plasma Fluid Equations from Collisional Kinetic Theory, Frontiers in Astronomy and Space Sciences, 11, https://doi.org/10.3389/fspas.2024.1466909, 2024.

Dimant, Y. S. and Oppenheim, M. M.: Ion Thermal Effects on E-region Instabilities: Linear Theory, Journal of Atmospheric and Solar-Terrestrial Physics, 66, 1639–1654, https://doi.org/10.1016/j.jastp.2004.07.006, 2004.

Dimant, Y. S. and Sudan, R. N.: Kinetic Theory of the Farley-Buneman Instability in the *E* Region of the Ionosphere, Journal of Geophysical Research: Space Physics, 100, 14 605–14 623, https://doi.org/10.1029/95JA00794, 1995.

Dimant, Y. S. and Sudan, R. N.: Physical Nature of a New Cross-field Current-driven Instability in the Lower Ionosphere, Journal of Geophysical Research: Space Physics, 102, 2551–2563, https://doi.org/10.1029/96JA03274, 1997.

Dimant, Y. S., Khazanov, G. V., and Oppenheim, M. M.: Effects of Electron Precipitation on E-Region Instabilities: Theoretical Analysis, Journal of Geophysical Research: Space Physics, 126, e2021JA029 884, https://doi.org/10.1029/2021JA029884, 2021.

Drexler, J., St. -Maurice, J.-P., Chen, D., and Moorcroft, D. R.: New Insights from a Nonlocal Generalization of the Farley-Buneman Instability Problem at High Latitudes, Annales Geophysicae, 20, 2003–2025, https://doi.org/10.5194/angeo-20-2003-2002, 2002.

Drossel, B.: Strong Emergence in Condensed Matter Physics, in: Top-Down Causation and Emergence, edited by Voosholz, J. and Gabriel, M., pp. 79–99, Springer International Publishing, Cham, ISBN 978-3-030-71899-2, https://doi.org/10.1007/978-3-030-71899-2_4, 2021.

Fang, X., Randall, C. E., Lummerzheim, D., Wang, W., Lu, G., Solomon, S. C., and Frahm, R. A.: Parameterization of Monoenergetic Electron Impact Ionization, Geophysical Research Letters, 37, https://doi.org/10.1029/2010GL045406, 2010.

Farley, D. T.: A Plasma Instability Resulting in Field-Aligned Irregularities in the Ionosphere, Journal of Geophysical Research (1896-1977), 68, 6083–6097, https://doi.org/10.1029/JZ068i022p06083, 1963.

Fejer, B. G. and Kelley, M. C.: Ionospheric Irregularities, Reviews of Geophysics, 18, 401–454, https://doi.org/10.1029/RG018i002p00401, 1980.

Foster, J. C. and Erickson, P. J.: Simultaneous Observations of E-region Coherent Backscatter and Electric Field Amplitude at F-region Heights with the Millstone Hill UHF Radar, Geophysical Research Letters, 27, 3177–3180, https://doi.org/10.1029/2000GL000042, 2000.

Foster, J. C. and Tetenbaum, D.: Phase Velocity Studies of 34-Cm *E*-Region Irregularities Observed at Millstone Hill, Journal of Atmospheric and Terrestrial Physics, 54, 759–768, https://doi.org/10.1016/0021-9169(92)90114-Z, 1992.

Foster, J. C., Tetenbaum, D., del Pozo, C. F., St-Maurice, J. P., and Moorcroft, D. R.: Aspect Angle Variations in Intensity, Phase Velocity, and Altitude for High-Latitude 34-Cm E Region Irregularities, Journal of Geophysical Research: Space Physics, 97, 8601–8617, https://doi.org/10.1029/91JA03144, 1992.

Fujii, R., Amm, O., Yoshikawa, A., Ieda, A., and Vanhamäki, H.: Reformulation and Energy Flow of the Cowling Channel, Journal of Geophysical Research: Space Physics, 116, https://doi.org/10.1029/2010JA015989, 2011.

Gillies, D. M., Liang, J., Donovan, E., and Spanswick, E.: The Apparent Motion of STEVE and the Picket Fence Phenomena, Geophysical Research Letters, 47, e2020GL088 980, https://doi.org/10.1029/2020GL088980, 2020.

Hall, G. E., MacDougall, J. W., Moorcroft, D. R., St.-Maurice, J.-P., Manson, A. H., and Meek, C. E.: Super Dual Auroral Radar Network Observations of Meteor Echoes, Journal of Geophysical Research: Space Physics, 102, 14 603–14 614, https://doi.org/10.1029/97JA00517, 1997.

Hamza, A. M.: Mode-Coupling and Nonlinear Landau Damping Effects in Auroral Farley-Buneman Turbulence, Journal of Nonlinear Mathematical Physics, 5, 438–461, https://doi.org/10.2991/jnmp.1998.5.4.9, 1998.

https://doi.org/10.5194/egusphere-2026-2345
Preprint. Discussion started: 21 May 2026

Hamza, A. M. and St-Maurice, J. P.: A Turbulent Theoretical Framework for the Study of Current-Driven E Region Irregularities at High Latitudes: Basic Derivation and Application to Gradient-Free Situations, Journal of Geophysical Research: Space Physics, 98, 11 587–11 599, https://doi.org/10.1029/92JA02836, 1993.

Harada, T. and Sasa, S.-i.: Equality Connecting Energy Dissipation with a Violation of the Fluctuation-Response Relation, Physical Review Letters, 95, 130 602, https://doi.org/10.1103/PhysRevLett.95.130602, 2005.

Hohenberg, P. C. and Halperin, B. I.: Theory of Dynamic Critical Phenomena, Reviews of Modern Physics, 49, 435–479, https://doi.org/10.1103/RevModPhys.49.435, 1977.

Huba, J. D., Hassam, A. B., Schwartz, I. B., and Keskinen, M. J.: Ionospheric Turbulence: Interchange Instabilities and Chaotic Fluid Behavior, Geophysical Research Letters, 12, 65–68, https://doi.org/10.1029/GL012i001p00065, 1985.

Hussey, G. C., Meek, C. E., André, D., Manson, A. H., Sofko, G. J., and Hall, C. M.: A Comparison of Northern Hemisphere Winds Using SuperDARN Meteor Trail and MF Radar Wind Measurements, Journal of Geophysical Research: Atmospheres, 105, 18 053–18 066, https://doi.org/10.1029/2000JD900272, 2000.

Huyghebaert, D., Hussey, G., Vierinen, J., McWilliams, K., and St-Maurice, J.-P.: ICEBEAR: An All-Digital Bistatic Coded Continuous-Wave Radar for Studies of the E Region of the Ionosphere, Radio Science, 54, 349–364, https://doi.org/10.1029/2018RS006747, 2019.

Huyghebaert, D., St.-Maurice, J.-P., McWilliams, K., Hussey, G., Howarth, A. D., Rutledge, P., and Erion, S.: The Properties of ICEBEAR E-Region Coherent Radar Echoes in the Presence of Near Infrared Auroral Emissions, as Measured by the Swarm-E Fast Auroral Imager, Journal of Geophysical Research: Space Physics, 126, e2021JA029 857, https://doi.org/10.1029/2021JA029857, 2021.

Ivarsen, M. F.: A Source or a Sink? How the Altitude of Particle Precipitation Influence High-Latitude Electrodynamics, Annales Geophysicae, 44, 149–162, https://doi.org/10.5194/angeo-44-149-2026, 2026.

Ivarsen, M. F., St-Maurice, J.-P., Hussey, G. C., Galeschuk, D., Lozinsky, A., Pitzel, B., and McWilliams, K. A.: An Algorithm to Separate Ionospheric Turbulence Radar Echoes From Those of Meteor Trails in Large Data Sets, Journal of Geophysical Research: Space Physics, 128, e2022JA031 050, https://doi.org/10.1029/2022JA031050, 2023.

Ivarsen, M. F., Gillies, M. D., Huyghebaert, D. R., St-Maurice, J.-P., Lozinsky, A., Galeschuk, D., Donovan, E., and Hussey, G. C.: Turbulence Embedded Into the Ionosphere by Electromagnetic Waves, Journal of Geophysical Research: Space Physics, 129, e2023JA032 310, https://doi.org/10.1029/2023JA032310, 2024a.

Ivarsen, M. F., Huyghebaert, D. R., Gillies, M. D., St-Maurice, J.-P., Themens, D. R., Oppenheim, M., Gustavsson, B. J., Billett, D., Pitzel, B., Galeschuk, D., Donovan, E., and Hussey, G. C.: Turbulence Around Auroral Arcs, Journal of Geophysical Research: Space Physics, 129, e2023JA032 309, https://doi.org/10.1029/2023JA032309, 2024b.

Ivarsen, M. F., St-Maurice, J.-P., Hussey, G. C., Huyghebaert, D. R., and Gillies, M. D.: Point-Cloud Clustering and Tracking Algorithm for Radar Interferometry, Physical Review E, 110, 045 207, https://doi.org/10.1103/PhysRevE.110.045207, 2024c.

Ivarsen, M. F., Miyashita, Y., St-Maurice, J.-P., Hussey, G. C., Pitzel, B., Galeschuk, D., Marei, S., Horne, R. B., Kasahara, Y., Matsuda, S., Kasahara, S., Keika, K., Miyoshi, Y., Yamamoto, K., Shinbori, A., Huyghebaert, D. R., Matsuoka, A., Yokota, S., and Tsuchiya, F.: Characteristic E-Region Plasma Signature of Magnetospheric Wave-Particle Interactions, Physical Review Letters, 134, 145 201, https://doi.org/10.1103/PhysRevLett.134.145201, 2025a.

Ivarsen, M. F., St-Maurice, J.-P., Hussey, G. C., Billet, D., Huyghebaert, D. R., Jin, Y., Miyashita, Y., Kasahara, S., Song, K., Jayachandran, P. T., Yokota, S., Miyoshi, Y., Yamamoto, K., Shinbori, A., Kasahara, Y., Shinohara, I., and Matsuoka, A.: Eastward Transients in the Dayside Ionosphere. I. Electrodynamics on Closed Field Lines, Physical Review E, 112, 045 204, https://doi.org/10.1103/r6bv-pzlq, 2025b.

https://doi.org/10.5194/egusphere-2026-2345
Preprint. Discussion started: 21 May 2026

Ivarsen, M. F., St-Maurice, J.-P., Hussey, G. C., McWilliams, K., Jin, Y., Huyghebaert, D. R., Miyashita, Y., and Sibeck, D.: Eastward Transients in the Dayside Ionosphere. II. A Parallel-Plate Capacitorlike Effect, Physical Review E, 112, 045 203, https://doi.org/10.1103/3bzj-bsf8, 2025c.

Jones, C. K. R. T.: Geometric Singular Perturbation Theory, vol. 1609, pp. 44–118, Springer Berlin Heidelberg, Berlin, Heidelberg, ISBN 978-3-540-60047-3 978-3-540-49415-7, https://doi.org/10.1007/BFb0095239, 1995.

Kasahara, S., Miyoshi, Y., Yokota, S., Mitani, T., Kasahara, Y., Matsuda, S., Kumamoto, A., Matsuoka, A., Kazama, Y., Frey, H. U., Angelopoulos, V., Kurita, S., Keika, K., Seki, K., and Shinohara, I.: Pulsating Aurora from Electron Scattering by Chorus Waves, Nature, 554, 337–340, https://doi.org/10.1038/nature25505, 2018a.

Kasahara, S., Yokota, S., Mitani, T., Asamura, K., Hirahara, M., Shibano, Y., and Takashima, T.: Medium-Energy Particle Experiments—Electron Analyzer (MEP-e) for the Exploration of Energization and Radiation in Geospace (ERG) Mission, Earth, Planets and Space, 70, 69, https://doi.org/10.1186/s40623-018-0847-z, 2018b.

Kasahara, Y., Kasaba, Y., Kojima, H., Yagitani, S., Ishisaka, K., Kumamoto, A., Tsuchiya, F., Ozaki, M., Matsuda, S., Imachi, T., Miyoshi, Y., Hikishima, M., Katoh, Y., Ota, M., Shoji, M., Matsuoka, A., and Shinohara, I.: The Plasma Wave Experiment (PWE) on Board the Arase (ERG) Satellite, Earth, Planets and Space, 70, 86, https://doi.org/10.1186/s40623-018-0842-4, 2018c.

Kaufman, H. R.: Explanation of Bohm Diffusion, Journal of Vacuum Science & Technology B: Microelectronics Processing and Phenomena, 8, 107–108, https://doi.org/10.1116/1.584855, 1990.

Kazama, Y., Wang, B.-J., Wang, S.-Y., Ho, P. T. P., Tam, S. W. Y., Chang, T.-F., Chiang, C.-Y., and Asamura, K.: Low-Energy Particle Experiments–Electron Analyzer (LEPe) Onboard the Arase Spacecraft, Earth, Planets and Space, 69, 165, https://doi.org/10.1186/s40623-017-0748-6, 2017.

Kelley, M. C., LaBelle, J., Kudeki, E., Fejer, B. G., Basu, Sa., Basu, Su., Baker, K. D., Hanuise, C., Argo, P., Woodman, R. F., Swartz, W. E., Farley, D. T., and Meriwether, J. W.: The Condor Equatorial Spread *F* Campaign: Overview and Results of the Large-scale Measurements, Journal of Geophysical Research: Space Physics, 91, 5487–5503, https://doi.org/10.1029/JA091iA05p05487, 1986a.

Kelley, M. C., Pfaff, R. F., and Haerendel, G.: Electric Field Measurements during the Condor Critical Velocity Experiment, Journal of Geophysical Research: Space Physics, 91, 9939–9946, https://doi.org/10.1029/JA091iA09p09939, 1986b.

Koustov, A. V., Danskin, D. W., Makarevitch, R. A., and Gorin, J. D.: On the Relationship between the Velocity of E-region HF Echoes and *ExB* Plasma Drift, Annales Geophysicae, 23, 371–378, https://doi.org/10.5194/angeo-23-371-2005, 2005.

Krommes, J. A.: Fundamental Statistical Descriptions of Plasma Turbulence in Magnetic Fields, Physics Reports, 360, 1–352, https://doi.org/10.1016/S0370-1573(01)00066-7, 2002.

Kumar, K. K.: Temperature Profiles in the MLT Region Using Radar-Meteor Trail Decay Times: Comparison with TIMED/SABER Observations, Geophysical Research Letters, 34, https://doi.org/10.1029/2007GL030704, 2007.

Loi, D., Mossa, S., and Cugliandolo, L. F.: Effective Temperature of Active Complex Matter, Soft Matter, 7, 3726–3729, https://doi.org/10.1039/C0SM01484B, 2011.

Lozinsky, A., Hussey, G., McWilliams, K., Huyghebaert, D., and Galeschuk, D.: ICEBEAR-3D: A Low Elevation Imaging Radar Using a Non-Uniform Coplanar Receiver Array for E Region Observations, Radio Science, 57, e2021RS007 358, https://doi.org/10.1029/2021RS007358, 2022.

Matsuoka, A., Teramoto, M., Nomura, R., Nosé, M., Fujimoto, A., Tanaka, Y., Shinohara, M., Nagatsuma, T., Shiokawa, K., Obana, Y., Miyoshi, Y., Mita, M., Takashima, T., and Shinohara, I.: The ARASE (ERG) Magnetic Field Investigation, Earth, Planets and Space, 70, 43, https://doi.org/10.1186/s40623-018-0800-1, 2018.

https://doi.org/10.5194/egusphere-2026-2345
Preprint. Discussion started: 21 May 2026

Mitani, T., Takashima, T., Kasahara, S., Miyake, W., and Hirahara, M.: High-Energy Electron Experiments (HEP) Aboard the ERG (Arase) Satellite, Earth, Planets and Space, 70, 77, https://doi.org/10.1186/s40623-018-0853-1, 2018.

Miyoshi, Y., Oyama, S., Saito, S., Kurita, S., Fujiwara, H., Kataoka, R., Ebihara, Y., Kletzing, C., Reeves, G., Santolik, O., Clilverd, M., Rodger, C. J., Turunen, E., and Tsuchiya, F.: Energetic Electron Precipitation Associated with Pulsating Aurora: EISCAT and Van Allen Probe Observations, Journal of Geophysical Research: Space Physics, 120, 2754–2766, https://doi.org/10.1002/2014JA020690, 2015.

Miyoshi, Y., Hori, T., Shoji, M., Teramoto, M., Chang, T. F., Segawa, T., Umemura, N., Matsuda, S., Kurita, S., Keika, K., Miyashita, Y., Seki, K., Tanaka, Y., Nishitani, N., Kasahara, S., Yokota, S., Matsuoka, A., Kasahara, Y., Asamura, K., Takashima, T., and Shinohara, I.: The ERG Science Center, Earth, Planets and Space, 70, 96, https://doi.org/10.1186/s40623-018-0867-8, 2018a.

Miyoshi, Y., Shinohara, I., Takashima, T., Asamura, K., Higashio, N., Mitani, T., Kasahara, S., Yokota, S., Kazama, Y., Wang, S.-Y., Tam, S. W. Y., Ho, P. T. P., Kasahara, Y., Kasaba, Y., Yagitani, S., Matsuoka, A., Kojima, H., Katoh, Y., Shiokawa, K., and Seki, K.: Geospace Exploration Project ERG, Earth, Planets and Space, 70, 101, https://doi.org/10.1186/s40623-018-0862-0, 2018b.

Miyoshi, Y., Hosokawa, K., Kurita, S., Oyama, S.-I., Ogawa, Y., Saito, S., Shinohara, I., Kero, A., Turunen, E., Verronen, P. T., Kasahara, S., Yokota, S., Mitani, T., Takashima, T., Higashio, N., Kasahara, Y., Matsuda, S., Tsuchiya, F., Kumamoto, A., Matsuoka, A., Hori, T., Keika, K., Shoji, M., Teramoto, M., Imajo, S., Jun, C., and Nakamura, S.: Penetration of MeV Electrons into the Mesosphere Accompanying Pulsating Aurorae, Scientific Reports, 11, 13 724, https://doi.org/10.1038/s41598-021-92611-3, 2021.

Miyoshi, Y., Shinohara, I., Ukhorskiy, S., Claudepierre, S. G., Mitani, T., Takashima, T., Hori, T., Santolik, O., Kolmasova, I., Matsuda, S., Kasahara, Y., Teramoto, M., Katoh, Y., Hikishima, M., Kojima, H., Kurita, S., Imajo, S., Higashio, N., Kasahara, S., Yokota, S., Asamura, K., Kazama, Y., Wang, S.-Y., Jun, C.-W., Kasaba, Y., Kumamoto, A., Tsuchiya, F., Shoji, M., Nakamura, S., Kitahara, M., Matsuoka, A., Shiokawa, K., Seki, K., Nosé, M., Takahashi, K., Martinez-Calderon, C., Hospodarsky, G., Colpitts, C., Kletzing, C., Wygant, J., Spence, H., Baker, D. N., Reeves, G. D., Blake, J. B., and Lanzerotti, L.: Collaborative Research Activities of the Arase and Van Allen Probes, Space Science Reviews, 218, 38, https://doi.org/10.1007/s11214-022-00885-4, 2022.

Newell, P. T. and Gjerloev, J. W.: Evaluation of SuperMAG Auroral Electrojet Indices as Indicators of Substorms and Auroral Power, Journal of Geophysical Research: Space Physics, 116, https://doi.org/10.1029/2011JA016779, 2011a.

Newell, P. T. and Gjerloev, J. W.: Substorm and Magnetosphere Characteristic Scales Inferred from the SuperMAG Auroral Electrojet Indices, Journal of Geophysical Research: Space Physics, 116, https://doi.org/10.1029/2011JA016936, 2011b.

Nishimura, Y., Lessard, M. R., Katoh, Y., Miyoshi, Y., Grono, E., Partamies, N., Sivadas, N., Hosokawa, K., Fukizawa, M., Samara, M., Michell, R. G., Kataoka, R., Sakanoi, T., Whiter, D. K., Oyama, S.-i., Ogawa, Y., and Kurita, S.: Diffuse and Pulsating Aurora, Space Science Reviews, 216, 4, https://doi.org/10.1007/s11214-019-0629-3, 2020.

Oppenheim, M., Otani, N., and Ronchi, C.: Hybrid Simulations of the Saturated Farley-Buneman Instability in the Ionosphere, Geophysical Research Letters, 22, 353–356, https://doi.org/10.1029/94GL03277, 1995.

Oppenheim, M., Otani, N., and Ronchi, C.: Saturation of the Farley-Buneman Instability via Nonlinear Electron E×B Drifts, Journal of Geophysical Research: Space Physics, 101, 17 273–17 286, https://doi.org/10.1029/96JA01403, 1996.

Oppenheim, M. M. and Dimant, Y. S.: Kinetic Simulations of 3-D Farley-Buneman Turbulence and Anomalous Electron Heating, Journal of Geophysical Research: Space Physics, 118, 1306–1318, https://doi.org/10.1002/jgra.50196, 2013.

Oppenheim, M. M., Dyrud, L. P., and vom Endt, A. F.: Plasma Instabilities in Meteor Trails: 2-D Simulation Studies, Journal of Geophysical Research: Space Physics, 108, https://doi.org/10.1029/2002JA009549, 2003.

Ott, T. and Bonitz, M.: Diffusion in a Strongly Coupled Magnetized Plasma, Physical Review Letters, 107, 135 003, https://doi.org/10.1103/PhysRevLett.107.135003, 2011.

https://doi.org/10.5194/egusphere-2026-2345
Preprint. Discussion started: 21 May 2026

Palmer, T. N.: Towards the Probabilistic Earth-system Simulator: A Vision for the Future of Climate and Weather Prediction, Quarterly Journal of the Royal Meteorological Society, 138, 841–861, https://doi.org/10.1002/qj.1923, 2012.

Pfaff, R. F., Kelley, M. C., Kudeki, E., Fejer, B. G., and Baker, K. D.: Electric Field and Plasma Density Measurements in the Strongly Driven Daytime Equatorial Electrojet: 2. Two-stream Waves, Journal of Geophysical Research: Space Physics, 92, 13 597–13 612, https://doi.org/10.1029/JA092iA12p13597, 1987.

Phythian, R.: Further Application of the Martin, Siggia, Rose Formalism, Journal of Physics A: Mathematical and General, 9, 269, https://doi.org/10.1088/0305-4470/9/2/012, 1976.

Roble, R. G., Ridley, E. C., Richmond, A. D., and Dickinson, R. E.: A Coupled Thermosphere/Ionosphere General Circulation Model, Geophysical Research Letters, 15, 1325–1328, https://doi.org/10.1029/GL015i012p01325, 1988.

Schlegel, K. and St.-Maurice, J. P.: Anomalous Heating of the Polar E Region by Unstable Plasma Waves 1. Observations, Journal of Geophysical Research: Space Physics, 86, 1447–1452, https://doi.org/10.1029/JA086iA03p01447, 1981.

Shen, Y., Verkhoglyadova, O. P., Artemyev, A., Hartinger, M. D., Angelopoulos, V., Shi, X., and Zou, Y.: Magnetospheric Control of Ionospheric TEC Perturbations via Whistler-Mode and ULF Waves, AGU Advances, 5, e2024AV001 302, https://doi.org/10.1029/2024AV001302, 2024.

Smagorinsky, J.: GENERAL CIRCULATION EXPERIMENTS WITH THE PRIMITIVE EQUATIONS: I. THE BASIC EXPERIMENT, Monthly Weather Review, 91, 99–164, https://doi.org/10.1175/1520-0493(1963)091<0099:GCEWTP>2.3.CO;2, 1963.

St. -Maurice, J.-P., Foster, J. C., Holt, J. M., and Del Pozo, C.: First Results on the Observation of 440-MHz High-Latitude Coherent Echoes from the E Region with the Millstone Hill Radar, Journal of Geophysical Research: Space Physics, 94, 6771–6798, 1989.

St.-Maurice, J.-P.: A Nonlocal Theory of the High-Latitude Farley-Buneman Instability, Journal of Geophysical Research: Space Physics, 90, 5211–5225, https://doi.org/10.1029/JA090iA06p05211, 1985.

St.-Maurice, J.-P. and Chau, J. L.: A Theoretical Framework for the Changing Spectral Properties of Meter-Scale Farley-Buneman Waves between 90 and 125 Km Altitudes, Journal of Geophysical Research: Space Physics, 121, 10,341–10,366, https://doi.org/10.1002/2016JA023105, 2016.

St-Maurice, J.-P. and Goodwin, L.: Revisiting the Behavior of the E-Region Electron Temperature During Strong Electric Field Events at High Latitudes, Journal of Geophysical Research: Space Physics, 126, 2020JA028 288, https://doi.org/10.1029/2020JA028288, 2021.

St.-Maurice, J.-P. and Hamza, A. M.: A New Nonlinear Approach to the Theory of E Region Irregularities, Journal of Geophysical Research: Space Physics, 106, 1751–1759, https://doi.org/10.1029/2000JA000246, 2001.

St-Maurice, J. P., Kofman, W., and Kluzek, E.: Electron Heating by Plasma Waves in the High Latitude E-region and Related Effects: Observations, Advances in Space Research, 10, 225–237, https://doi.org/10.1016/0273-1177(90)90256-Y, 1990.

St-Maurice, J.-P., Huyghebaert, D., Ivarsen, M. F., and Hussey, G. C.: Narrow Width Farley-Buneman Spectra Above 100 Km Altitude, Journal of Geophysical Research: Space Physics, 128, e2022JA031 191, https://doi.org/10.1029/2022JA031191, 2023.

Stewart, W. C.: Current-Voltage Characteristics of Josephson Junctions, Applied Physics Letters, 12, 277–280, https://doi.org/10.1063/1.1651991, 1968.

Thorne, R. M., Ni, B., Tao, X., Horne, R. B., and Meredith, N. P.: Scattering by Chorus Waves as the Dominant Cause of Diffuse Auroral Precipitation, Nature, 467, 943–946, https://doi.org/10.1038/nature09467, 2010.

Treumann, R. A. and Baumjohann, W.: Advanced Space Plasma Physics, vol. 30, Imperial College Press London, 1997.

Vaishnav, R., Jacobi, C., Berdermann, J., Codrescu, M., and Schmölter, E.: Role of Eddy Diffusion in the Delayed Ionospheric Response to Solar Flux Changes, Annales Geophysicae, 39, 641–655, https://doi.org/10.5194/angeo-39-641-2021, 2021.

https://doi.org/10.5194/egusphere-2026-2345
Preprint. Discussion started: 21 May 2026

Watt, C. E. J., Allison, H. J., Bentley, S. N., Thompson, R. L., Rae, I. J., Allanson, O., Meredith, N. P., Ross, J. P. J., Glauert, S. A., Horne, R. B., Zhang, S., Murphy, K. R., Rasinskaitė, D., and Killey, S.: Temporal Variability of Quasi-Linear Pitch-Angle Diffusion, Frontiers in Astronomy and Space Sciences, 9, https://doi.org/10.3389/fspas.2022.1004634, 2022.

Wiesenfeld, K.: New Results on Frequency-Locking Dynamics of Disordered Josephson Arrays, Physica B: Condensed Matter, 222, 315–319, https://doi.org/10.1016/0921-4526(96)85057-5, 1996.

Wiesenfeld, K., Colet, P., and Strogatz, S. H.: Synchronization Transitions in a Disordered Josephson Series Array, Physical Review Letters, 76, 404–407, https://doi.org/10.1103/PhysRevLett.76.404, 1996.

Wilson, K. G.: Renormalization Group and Critical Phenomena. I. Renormalization Group and the Kadanoff Scaling Picture, Physical Review B, 4, 3174–3183, https://doi.org/10.1103/PhysRevB.4.3174, 1971.

Wiltberger, M., Merkin, V., Zhang, B., Toffoletto, F., Oppenheim, M., Wang, W., Lyon, J. G., Liu, J., Dimant, Y., Sitnov, M. I., and Stephens, G. K.: Effects of Electrojet Turbulence on a Magnetosphere-Ionosphere Simulation of a Geomagnetic Storm, Journal of Geophysical Research: Space Physics, 122, 5008–5027, https://doi.org/10.1002/2016JA023700, 2017a.

Wiltberger, M., Rigler, E. J., Merkin, V., and Lyon, J. G.: Structure of High Latitude Currents in Magnetosphere-Ionosphere Models, Space Science Reviews, 206, 575–598, https://doi.org/10.1007/s11214-016-0271-2, 2017b.

Wu, Q., Schreiner, W. S., Ho, S.-P., Liu, H.-L., and Qian, L.: Observations and Simulations of Eddy Diffusion and Tidal Effects on the Semiannual Oscillation in the Ionosphere, Journal of Geophysical Research: Space Physics, 122, 10,502–10,510, https://doi.org/10.1002/2017JA024341, 2017.